Technical Memorandum No. 295

Offline validation of the ERA40 surface scheme

Bart van den Hurk
Pedro Viterbo
Anton Beljaars
Alan Betts

Research Department

January 2000

Offline validation of the ERA40 surface scheme

B.J.J.M. van den Hurk[1], P. Viterbo[2], A.C.M. Beljaars[2] and A.K. Betts[3]

[1] *Royal Netherlands Meteorological Institute, De Bilt The Netherlands*
[2] *European Centre for Medium-Range Weather Forecasts, Reading, UK*
[3] *Atmospheric Research, Pittsford, Vermont, USA*

Abstract

A new surface scheme is introduced in the upcoming ECMWF global reanalysis covering a 40-year period 1957-1997 (known as ERA40). The new scheme is characterized by a tiled treatment of subgrid fractions of evaporating surfaces, the use of a global vegetation database plus an associated set of model parameters, and changes into the parameterization of snow processes, the coupling of the skin layer to the soil, and the vertical soil moisture transport.

Parallel to the evaluation of the global impact in the ECMWF 3D model, this tiled scheme was tested in offline mode with data from 7 long term surface field campaigns. The datasets cover a wide range of climate regions and surface land use and vegetation types, ranging from boreal (BOREAS), tropical (ARME) and temperate (Garderen) forest, via savannah (SEBEX) and prairie (FIFE) to crop (HAPEX-Mobilhy) and grassland (Cabauw).

The offline evaluation was primarily used for validation purposes, but gave also rise to adjusting parameter settings and/or parameterization approaches. After the combined calibration/validation exercise we can conclude that (a) the description of snow processes and surface fluxes in the Boreal areas has improved significantly, (b) the tiling approach does not give rise to major changes in the model correspondence to data in case of grass- and cropland, and (c) model performance becomes increasingly dependent on a proper choice of vegetation dependent model parameters, which gives rise to an increased number of degrees of freedom.

1 Introduction

Several recent studies revealed some persistent problems with the land surface parameterization scheme in the global model of the European Centre for Medium-range Weather Forecasts (ECMWF), published by Viterbo and Beljaars (1995), which we will refer to as VB95 hereafter. For instance, Van den Hurk and Beljaars (1996) found that the uniform skin temperature for all components in the grid box artificially enhanced canopy transpiration in a semi-arid vineyard area. Using results from the first ECMWF Re-Analysis (ERA15), Bosveld *et al.* (1998) observe among other features a too large diurnal cycle of the surface temperature for a grassland site near Cabauw, The Netherlands. Betts *et al.* (1998a) conclude that the soil hydrological cycle in the ERA15 database is adversely affected by the soil moisture nudging increments, described

by Viterbo (1994). This is also found by Douville *et al.* (1998) in a comparison with data from the Global Soil Wetness Project. They suggest that the lack of a realistic description of vegetation types is a serious shortcoming of the ERA15-system. Betts *et al.* (1998b) analyzed ERA15 results using data from both the First ISLSCP Field Experiment (FIFE, ISLSCP standing for International Satellite Land Surface Climatology Project) and the Boreal Ecosystem-Atmosphere Study (BOREAS). They concluded that the ERA15 land surface treatment resulted in too large evaporation rates over boreal forests both in winter and spring (due to the lack of reduction of root extraction in frozen soil) and summer (due to the absence of a stomatal control by atmospheric humidity deficit, found by Betts *et al.*, 1999). Surface runoff is virtually absent in the scheme of VB95, in contrast to observations on large catchments (Hagemann and Dümenil, 1999).

Also routine inspection of the ECMWF forecasts revealed possibilities for improvement of the original scheme of VB95. Heat release due to soil freezing had a major effect on near surface temperature bias in winter (Viterbo *et al.*, 1999). In order to increase turbulent heating of the atmosphere over boreal forests, the albedo of snow covered forests should be limited to a value of order 0.20, owing to the dark tree canopy elements which penetrate through the snow deck (Viterbo and Betts, 1999).

The ERA15 archive has proved to be very useful. Not only it made possible a thorough analysis of the skill and shortcomings of the global model over a long period, it also supported research activities related to climate change and long term atmospheric dynamics. A new reanalysis cycle is planned at ECMWF covering a 40-year period 1957-1997. Guided by the land surface studies mentioned above, and by many discussions — in particular in the context of the ECMWF/GEWEX workshop on modelling and data assimilation for land-surface processes, held at ECMWF between 29 June and 2 July 1998 — it was decided to redesign the land surface parameterization (LSP) scheme before starting a new 40-year reanalysis cycle (Viterbo *et al.*, 2000). The basic differences from the original LSP scheme are

- Grid box surface fluxes are calculated separately for the different subgrid surface fractions (or "tiles"), leading to a separate solution of the surface energy balance equation and skin temperature for each of these tiles. This is an analogue of the "mosaic" approach of Koster and Suarez (1992);

- The four already existing tiles (bare soil, vegetation, snow, interception layer) are replaced by 8 new tiles (bare soil, high vegetation, low vegetation, high vegetation with snow beneath, snow on low vegetation, interception layer, sea-ice, open water). For the moment, the distinction between water and land is still controlled by a land-sea mask, which implies that only six tiles are used over land, and two over sea;

- The global uniform vegetation is replaced by a coverage map of vegetation types, divided in 18 broad categories. LSP parameters vary per vegetation type;

- A new set of environmental controls on canopy transpiration is introduced, including the response to air humidity deficit and the lack of water extraction from frozen soils;

- On top of the soil, a new single snow layer is introduced. The snow scheme includes prognostic equations for albedo and density, and a separate energy balance equation for

high and low vegetation tiles with snow.

Prior to operational implementation of this new surface parameterization scheme it was evaluated in a number of experiments. Viterbo *et al.* (2000) discuss a comparison of the new scheme to the operational formulation for a series of simulations using the global forecast system, both the full 3D model including data assimilation and a special version allowing for a relaxation of the higher atmospheric layers to analyzed fields. Both types of experiments covered at least one complete seasonal cycle.

Parallel to these large scale interactive simulations, the new scheme was evaluated offline using a number of validation data sets. The offline simulations were executed by forcing the LSP scheme by an observed continuous time series of downward long wave and short wave radiation, precipitation, wind speed, temperature, air humidity and air pressure, and comparing the calculations to observed fluxes and state variables. Although interactions between the land surface scheme and other components of the atmospheric model cannot be examined, these offline simulations have proven to be very useful in past model designs and evaluations (see, e.g. VB95 and the results of the Project for Intercomparison of Land-surface Intercomparison Schemes PILPS, Henderson-Sellers *et al.*, 1993).

This offline evaluation was carried out using results of 7 long-term measurement campaigns, each within a different climate zone and with a different surface type. Some of these datasets and forcing records were used for testing of the original model (VB95). For one site (the BOREAS site) a new forcing and validation dataset was constructed using data from several sources, while the forcing record of the FIFE site was extended from 6 to nearly 30 months using a merge of data from the local measurement campaign and ERA15 radiation data for the same location.

Both the operational ECMWF surface scheme (based on VB95) and the new version were subjected to this offline evaluation. The purpose of the simulations was twofold. First, field data were used for limited calibration of some of the many new coefficients. Second, it allows an assessment of the improvement of the new scheme compared to the operational one, guided by ground truth data, if possible.

This paper describes the main results of the offline evaluation of the new surface scheme. Although a full description of the new scheme can be found elsewhere (Viterbo *et al.*, 2000), a basic outline of the new scheme will be presented here. Also the forcing and validation data sets will be described briefly, before adressing the results and conclusions.

2 Brief description of the new surface model

Viterbo *et al.* (2000) give a full description of the new surface model. Owing to the introduction of the separate solution of the energy balance of the different tiles, the new scheme will usually be denoted as the "tiled" surface scheme in the following. Since the treatment of vegetation and snow are the major novelties in the new scheme, these components will be described in some detail.

Table 1: Vegetation types and parameter values in the new model (see text). Also shown are relevant parameters in the control model (VB95). *H/L* refers to the distinction between high and low vegetation.

index	vegetation type	H/L	$r_{s,min}$	LAI	c_{veg}	g_D	a_r	b_r	z_{0v}
-	-	veg	s/m	m^2/m^2	-	mb^{-1}	-	-	m
1	Crops, Mixed Farming	L	180	3	0.90	0	5.558	2.614	0.10
2	Short Grass	L	110	2	0.85	0	10.739	2.608	0.05
3	Evergreen Needleleaf Trees	H	500	5	0.90	0.03	6.706	2.175	1.50
4	Deciduous Needleleaf Trees	H	500	5	0.90	0.03	7.066	1.953	1.50
5	Deciduous Broadleaf Trees	H	175	5	0.90	0.03	5.990	1.955	1.00
6	Evergreen Broadleaf Trees	H	240	6	0.99	0.03	7.344	1.303	2.00
7	Tall Grass	L	100	2	0.70	0	8.085	1.697	0.10
8	Desert	L	250	0.5	0.00	0	-	-	0.01
9	Tundra	L	80	1	0.50	0	8.992	8.992	0.05
10	Irrigated Crops	L	180	3	0.90	0	5.558	2.614	0.06
11	Semidesert	L	150	0.5	0.10	0	4.372	0.978	0.06
12	Ice Caps and Glaciers	-	-	-	-	-	-	-	-
13	Bogs and Marshes	L	240	4	0.60	0	7.344	1.303	0.03
14	Inland Water	-	-	-	-	-	-	-	
15	Ocean	-	-	-	-	-	-	-	
16	Evergreen Shrubs	L	225	3	0.50	0	6.326	1.567	0.10
17	Deciduous Shrubs	L	225	1.5	0.50	0	6.326	1.567	0.10
18	Mixed Forest/woodland	H	250	5	0.90	0.03	4.453	1.631	1.00
19	Interrupted Forest	H	175	2.5	0.90	0.03	4.453	1.631	1.00
20	Water and Land Mixtures	L	150	4	0.60	0	-	-	
-	Control model (VB95)	-	240*	4	-	0	see table 3		-

* In fact, the stress function to intercepted shortwave radiation in the old scheme differed by 13% from unity for high values of intercepted radiation. This implies that $r_{s,min}$, in the sense of a minimum resistance in absence of any stress, is effectively 272 s/m.

2.1 Tile parameters

Each grid box is divided into 8 fractions: two vegetated fractions (high and low vegetation without snow), one bare soil fraction, three snow/ice fractions (snow on bare ground/low vegetation, high vegetation with snow beneath, and sea-ice, respectively), and two water fractions (interception reservoir, ocean/lakes). The tile for "high vegetation with snow beneath" is a combined tile with a separate energy balance and evaporation model for the high vegetation and the underlying snow.

In each gridbox two vegetation types are present: a high and a low vegetation type. An external climate database, based on the USGS NOAA based global dataset (see USGS, 1999) is used to specify the vegetation type, VT_H and VT_L, and the area fraction, A_H and A_L, for each of the high and low vegetation components, respectively. Each vegetation type is characterized a by a series of (fixed) parameters (see table 1):

- A minimum canopy resistance $r_{s,min}$;
- A vegetation coverage c_{veg};

Table 2: Tile specific parameter values. The resistance scheme describes the way of coupling to the atmosphere: *potential* denotes aerodynamic resistance only; *resistance* denotes aerodynamic resistance in series with a canopy or soil resistance; *canopy and snow resistance* denotes a canopy resistance for the vegetation and an extra aerodynamic coupling to the snow surface (see figure 1). Unstable/stable refers to the temperature gradient between the skin layer and the top soil or snow layer. Also shown are relevant values for the control model of VB95.

Tile	Λ_{sk} $(Wm^{-2}K^{-1})$ unstable	stable	f_{Rs}	resistance scheme
high vegetation	20	9.5	0.03	resistance
low vegetation	10		0.05	resistance
high vegetation with snow beneath	20	9.5	0.03	canopy and snow resistance
snow on low vegetation	7		0	potential
bare ground	15		0	resistance
interception reservoir	10		0.05	resistance
ocean	∞		0	potential
sea ice	58		0	potential
control model (VB95)	15		0	mix

- A leaf area index LAI;
- A sensitivity coefficient g_D for the dependence of the canopy resistance r_c on water vapour pressure deficit;
- The root distribution over the soil layers, specified by an exponential profile involving attenuation coefficients a_r and b_r;
- A vegetation roughness length z_{0v}[1].

The vegetation types are based on the classification of the BATS surface scheme (Dickinson *et al.*, 1993), as given in the USGS (1999) dataset. The parameters are based both on experiments conducted as described below and on literature review, in particular Mahfouf *et al.* (1995), Manzi and Planton (1994), Giard and Bazile (1999), Dorman and Sellers (1989), Bonan (1994), Pitman *et al.* (1991) and Zeng *et al.* (1998). A further discussion on the parameter values can be found in Viterbo *et al.* (2000).

The coverage C_i for each of the tiles i depends on the type and relative area of low and high vegetation, and the presence of snow and intercepted water. In the absence of snow and interception, the vegetation coverage of high (c_H) and low (c_L) vegetation is calculated as $A_H \times c_{veg}(VT_H)$ and $A_L \times c_{veg}(VT_L)$, respectively, with c_{veg} a vegetation type dependent coverage (table 1). The bare ground fraction c_B is the residual.

[1] In the ECMWF global model, surface roughness is extracted from a global climate database. Here, we include the vegetation roughness length for the sake of specifying an appropriate roughness for each simulation site (see below). Extracting it from the global database would yield unrealistically high values, as orographic influences are blended into the database. The orographic contribution is not appropriate for the atmospheric forcings measured close to the surface as used here. However, including the vegetation roughness as listed in table 1 in the operational global model is foreseen in the near future.

Presence of snow and intercepted water dynamically modify the coverage fractions. The coverage of snow (c_s) is linearly related to the snow depth S_N. The interception reservoir fraction c_l is equivalently given by W_l/W_{lmax}, with W_{lmax} defined from the leaf area index contributions from the high and low vegetation tiles. Both W_l and S_N are prognostic quantities in the model. Snow cover is assumed to be overlying vegetation and bare ground with the same fraction. The interception reservoir occupies an identical fraction of all snow-free tiles. At present, the partial gridbox coverage by sea-ice and ocean/lakes is not (yet) implemented, and these will not be considered in the following.

Apart from the fractional gridbox coverage, each tile has a couple of additional parameters (see table 2):

- the skin conductivity Λ_{sk}, providing the thermal connection to the soil or snow deck. For high vegetation, Λ_{sk} is different for a stable and unstable stratification of the temperature gradient between the skin layer and the upper soil or snow layer. This difference is considered to represent the asymmetric coupling between the ground surface and the tree canopy layer: an effective convective transport within the tree trunk space for unstable conditions, and a limited turbulent exchange for stable stratification (Bosveld *et al.*, 1999);

- a small fraction f_{Rs} of net shortwave radiation that is transmitted directly to the top soil or snow layer. The remaining part of the shortwave radiation (1 - f_{Rs}) is absorbed by the skin layer.

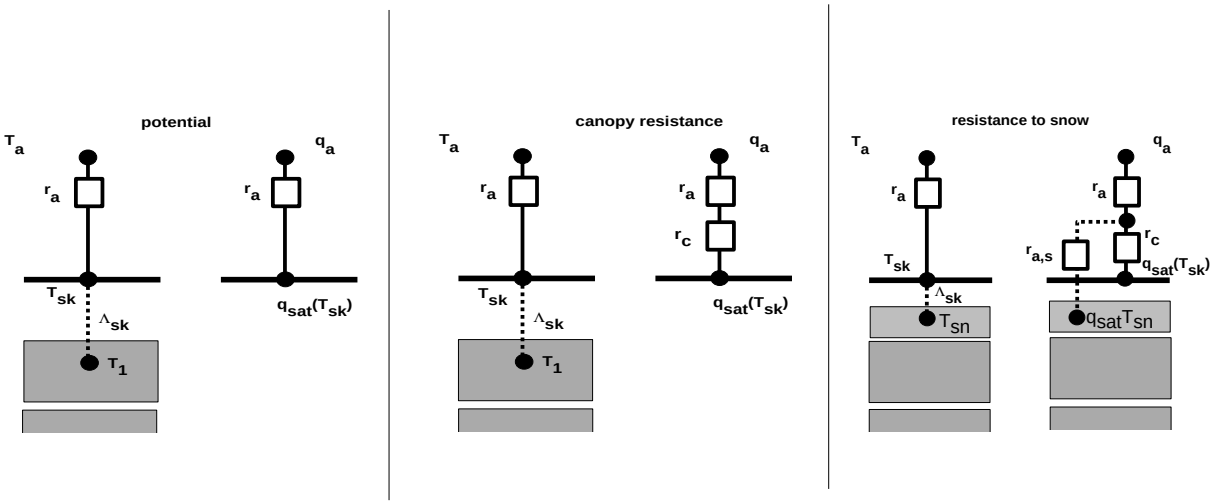

Figure 1: Resistance scheme for 3 categories of coupling. *potential* refers to ocean, sea ice and snow on low vegetation; *(canopy) resistance* to dry low and dry high vegetation, bare soil, and interception reservoir when potential evaporation exceeds the maximum reservoir content; *resistance to snow* to snow under high vegetation.

The surface albedo α is similar for all tiles except for those covered with snow (see the snow scheme description below). The climate database provides the snow free background albedo on a monthly basis. Long wave emissivity ε is equal to 0.99 for all tiles. All other surface characteristics (roughness length for momentum z_{0m} and heat z_{0h}, geopotential height) are similar for all tiles and specified in the climate database.

2.2 The coupling of the surface to the atmosphere

As in the previous model of VB95, a skin temperature T_{sk} forms the interface between the soil and the atmosphere. It is calculated for each of the grid box tiles separately. This is done by looping the surface energy balance solver over the 8 tiles, assuming a complete coverage of the specific tile. For a single tile, this procedure is very similar to the derivation of the Penman-Monteith equation in which the skin temperature is eliminated from the surface energy balance equation. The numerical approach as in the tile model has the advantage that the feedback of skin temperature on net radiation and ground heat flux is included. The input radiation and reference atmospheric temperature (T_a), specific humidity (q_a) and wind speed (U_a) are identical for each tile. The surface fluxes "seen" by the atmosphere are calculated as an area-weighted average over the tiles. For the high vegetation with snow underneath, the skin temperature is that of the high vegetation. The temperature of the underlying snow is calculated separately.

The energy balance equation solved for each tile is similar to the old scheme. The only difference from VB95 is the introduction of the partial absorption of net shortwave radiation, $1 - f_{Rs,i}$ in the skin layer (see table 2). The remaining energy is directly passed to the soil or snow:

$$(1-\alpha_i)(1-f_{Rs,i})R_s + \varepsilon(R_T - \sigma T_{sk,i}^4) + H_i + L_{v,s}E_i = \Lambda_{sk,i}(T_{sk,i} - T_1) \tag{1}$$

where i denotes the tile index. The symbols are R_s and R_T for downward shortwave and longwave radiation, respectively, σ is the Stefan-Bolzman constant, T_1 the temperature of the upper soil or snow layer, H_i the sensible heat flux, and $L_{v,s}E_i$ the latent heat flux from the skin layer. Latent heat for vaporization, L_v, is used for all evaporation terms not including snow evaporation, while L_s, the sublimation energy, is used for evaporation of snow.

As in the former model version, a resistance parameterization is used to calculate the turbulent fluxes. Momentum exchange is parameterized with the same roughness length for all tiles, but a different stability correction for each tile. The resistance scheme for water vapour and heat exchange is different for different tiles (see figure 1). For ocean, sea ice and snow on low vegetation, the turbulent exchange of heat and water vapour is given by

$$H_i = \rho_a c_p |U_a| C_{H,i} \left(T_a + gz - T_{sk,i}\right) \tag{2}$$

$$L_{v,s}E_i = \rho_a L_{v,s} |U_a| C_{H,i} \left(q_a - q_{sat}(T_{sk,i})\right) \tag{3}$$

with ρ_a the air density, c_p the heat capacity of dry air, g gravity acceleration, z height of lowest model level above the surface and $C_{H,i}$ the turbulent exchange coefficient. $C_{H,i}$ may vary from tile to tile because of differing atmospheric stability.

For high and low vegetation, an additional canopy resistance r_c is added:

$$L_v E_i = \frac{L_v \rho_a}{r_c + r_a} \left(q_a - q_{sat}(T_{sk,i})\right). \tag{4}$$

with $r_a \equiv (|U_a| C_{H,i})^{-1}$ and i indicating the high or low vegetation tiles. r_c is a function of downward shortwave radiation R_s, leaf area index LAI, average soil moisture content $\overline{\omega}$,

Table 3: Root distribution per vegetation type (in %) over the 4 layers. Vegetation indexes refer to table 1.

veg. index	old	1	2	3	4	5	6	7	8	9	10	11	13	16	17	18	19
layer 1	33	24	35	26	26	24	25	27	100	47	24	17	25	23	23	19	19
layer 2	33	41	38	39	38	38	34	37	0	45	41	31	34	36	36	35	35
layer 3	33	31	23	29	29	31	27	27	0	8	31	33	27	30	30	36	36
layer 4	0	4	4	6	7	7	14	9	0	0	4	19	14	11	11	10	10

atmospheric water vapour deficit D_a and a minimum stomatal resistance $r_{s,min}$, following Jarvis (1976):

$$r_c = \frac{r_{s,min}}{LAI} f_1(R_s) f_2(\overline{\omega}) f_3(D_a). \tag{5}$$

As explained in Viterbo *et al.* (2000), f_1 is a straightforward hyperbolic function of downward shortwave radiation only:

$$f_1(R_s)^{-1} = \min\left[1, \frac{a(1+bR_s)}{bR_s + c}\right] \tag{6}$$

where $a = 0.81$, $b = 0.004\ (W/m^2)^{-1}$ and $c = 0.05$.

Function f_2 follows the previous model version, but allows for frozen soil and for variability in the root extraction profile defining $\overline{\omega}$ (see table 3):

$$f_2(\overline{\omega})^{-1} = \begin{cases} 0 & \overline{\omega} < \omega_{pwp} \\ \frac{\overline{\omega}-\omega_{pwp}}{\omega_{cap}-\omega_{pwp}} & \omega_{pwp} \le \overline{\omega} < \omega_{cap} \\ 1 & \overline{\omega} \ge \omega_{cap} \end{cases} \tag{7}$$

$f_2(\overline{\omega})$ is calculated over the liquid part of the soil moisture only. The fraction of unfrozen soil water, f_{liq}, is a parameterized function of the soil temperature T_s (Viterbo *et al.*, 1999). In equation 7 $\overline{\omega}$ is thus defined as

$$\overline{\omega} = \sum_{k=1}^{4} R_k \max[f_{liq,k}\omega_k, \omega_{pwp}] \tag{8}$$

The soil coefficients ω_{pwp} and ω_{cap} are unchanged from VB95 (see table 4). Table 1 lists coefficients a_r and b_r which are used to calculate the root density R_k according to Zeng *et al.* (1998):

$$R_k = 0.5\left[\exp(-a_r z_{k-1}) + \exp(-b_r z_{k-1}) - \exp(-a_r z_k) - \exp(-b_r z_k)\right] \tag{9}$$

where z_k is the depth of the bottom of layer k (in m; $z_{k=0} = 0\ m$). Contributions from levels exceeding the column depth are added to the deepest soil layer in order to ensure that $\sum R_k = 1$. Table 3 lists the distribution of the roots over the 4 soil layers.

A dependence on atmospheric humidity deficit ($D_a \equiv e_{sat}(T_a) - e_a$, with e the vapour pressure) is included according to

$$f_3(D_a)^{-1} = \exp(-g_D D_a) \tag{10}$$

where g_D depends on the vegetation type (table 1) and exceeds zero for high vegetation only.

Evaporation from the interception reservoir is given by equation 3 only when the amount of water in the interception reservoir, W_l, is sufficient to sustain potential evaporation during the entire time step Δt. If W_l is limited, an additional resistance r_l, analogue to r_c in equation 4, is introduced. r_l is calculated from the potential evaporation in the previous timestep.

Bare soil evaporation is changed from a relative humidity expression in VB95 to a resistance approach, analogue to the canopy transpiration formulation (equation 4). The soil evaporation resistance, r_{soil}, is

$$r_{soil} = r_{soil,min} f_2(f_{liq,1}\omega_1) \tag{11}$$

with f_2 given by equation 7, and $r_{soil,min} = 50\ s/m$. By this parameterization, evaporation from bare ground is treated similar to a single leaved canopy with a minimum resistance $r_{soil,min}$, extracting water from the upper soil layer only, and not experiencing any additional stress due to limited radiation or dry air.

A special treatment is included in the calculation of evaporation over high vegetation with snow underneath (see figure 1). Evaporation takes place from both the canopy component in the tile (E_{veg}, following equation 4) and from the snow lying under the vegetation. The canopy evaporation uses a canopy resistance and saturation specific humidity at the canopy skin temperature, while the snow evaporation $L_s E_{snow}$ is parameterized with an additional constant aerodynamic resistance $r_{a,s}$ and saturation specific humidity at snow temperature T_{SN} (see below):

$$L_s E_{snow} = \frac{L_s \rho_a}{r_{a,s} + r_a} \left(q_a - q_{sat}(T_{SN})\right). \tag{12}$$

with $r_{a,s} = 100 s/m$. In Spring, $L_v E_{veg} + L_s E_{snow}$ will be dominated by snow evaporation since the frozen soil under the snow deck will lead to very large values of r_c.

The grid box total sensible and latent heat fluxes are now an area weighted average:

$$H_{grid} = \sum_{i=1}^{8} C_i H_i \tag{13}$$

$$E_{grid} = \sum_{i=1}^{8} C_i E_i \tag{14}$$

with C_i the respective grid box fractions, H_i given by equation 2, and E_i by equations 3 for ocean, sea-ice and snow on low vegetation, 4 for dry high and low vegetation, the interception reservoir (with r_c replaced by r_l) and for bare soil (with r_c replaced by r_{soil}) and a combination of equations 4 and 12 for high vegetation with underlying snow.

2.3 Coupling to the soil

As in the old scheme, the soil heat flux drives the soil temperature changes. Some differences compared to the old scheme are:

Table 4: Soil physical coefficients in the ECMWF surface scheme.

Parameter	units	meaning	value
γ_{sat}	m/s	hydraulic conductivity at saturation	4.57×10^{-6}
Ψ_{sat}	m	water pressure head at saturation	-0.346
b	-	Clapp and Hornberger (1978) coefficient	6.0
ω_{sat}	m^3/m^3	soil porosity	0.472
ω_{cap}	m^3/m^3	volumetric water content at field capacity	0.323
ω_{pwp}	m^3/m^3	volumetric water content at wilting point	0.171

- The tiled surface is coupled to a single soil profile. The net flux into the soil is a weighted average of the flux from each tile.

- From the snow free tiles, the flux into the soil consists of two parts. Apart from the diffusion of heat governed by $\Lambda_{sk,i}(T_{sk,i}-T_1)$ (equation 1), the residual of the net shortwave radiation not absorbed by the skin layer (f_{Rs}) provides energy to the soil. Table 2 lists the values for $\Lambda_{sk,i}$ and $f_{Rs,i}$ for each of the tiles.

- For the snow tiles, the heat flux into the soil is calculated using a resistance formulation:

$$G_{SN} = \frac{T_{SN} - T_1}{r_{snow}} \tag{15}$$

  with r_{snow} given by the sum of the resistance through half the snow layer and the reciprocal of the skin conductivity of bare ground.

The net heat flux into the soil is now given by:

$$G_{grid} = \sum_i C_i \left\{ \Lambda_{sk,i}(T_{sk,i} - T_1) + f_{Rs,i}(1-\alpha_i)R_s \right\} + c_s G_{SN} \tag{16}$$

where the summation loops over all snow free tiles.

Compared to the original model by VB95, the energy release or uptake of freezing or melting soil water (Viterbo *et al.*, 1999) is included in the soil thermal budget. Also, the dependence of the soil thermal conductivity on soil water content is changed following Peters-Lidard *et al.* (1997).

2.4 Soil moisture transport and root extraction

The vertical soil moisture transport is governed by infiltration, surface runoff, gradient diffusion, gravity and deep water percolation. The hydraulic diffusivity λ and conductivity γ are functions of the *liquid* soil water content $f_{liq} \times \omega$, and generic soil physical coefficients γ_{sat}, ω_{sat}, b and ψ_{sat} (see table 4).

Water removed from the soil by canopy transpiration is extracted from the soil layers using a weighing function. The weight includes the root density R_k and now, in contrast to VB95, avoids extraction from layers in which $f_{liq}\omega_k < \omega_{pwp}$, which reflects the preference of plants to extract water only from those layers where the liquid water content exceeds the wilting point.

2.5 The snow scheme

The snow scheme is now no longer merged into the upper soil layer, as in VB95, but represents an additional snow pack on top of the upper soil layer. The snow pack is represented by a single snow temperature, T_{SN} and thickness of the pack D_s. The net energy absorption in the snow pack per unit snow covered area, Q_{SN}, is the residual of the skin energy balance from the snow covered tiles and the snow evaporation from the tile with high vegetation over snow (equation 12). The heat loss to the soil, G_{SN}, is given by equation 15. The absorbed energy Q_{SN} is used to change the snow temperature or melt the snow, when T_{SN} exceeds the melting point.

The heat capacity of the snow deck is a function of its depth and the snow density, which is a prognostic quantity depending on snow age following Douville *et al.* (1995). The snow thermal conductivity changes with changing snow density. The snow albedo changes exponentially with snow age. For snow on low vegetation it ranges between 0.50 for old snow and 0.85 for fresh snow (to which it is reset whenever the snow fall exceeds 1 mm/hr). The albedo for high vegetation with snow underneath is fixed at 0.15.

2.6 Simulation strategy

For all available sites at least two model runs were executed: a *control* simulation with the operational code, and a simulation with the *tiled* model version. Surface characteristics were found from the closest grid point in the global surface climate database. An exception to this was the specification of SEBEX, which site is located in a strong north-south gradient with surface characteristics ranging from desert (in the database at the actual SEBEX location) to tall grass. The latter surface type is most appropriate for the site conditions, and we chose the closest grid point with this surface type from the database.

In order to avoid large roughness lengths including orographic contributions, as included in the global database, a site specific roughness length was computed from the vegetation roughness listed in table 1. Following Claussen *et al.* (1994), a blended roughness z_{0m} is calculated as

$$\frac{1}{\ln^2\left(\frac{z_b}{z_{0m}}\right)} = \sum_i \frac{C_i}{\ln^2\left(\frac{z_b}{z_{0v,i}}\right)} \tag{17}$$

where a blending height z_b of 100 m is chosen, and the summation is over the vegetation and bare ground fractions without snow or interception. The bare ground roughness length is assumed to be 0.01 m, while $z_{0v,i}$ is as prescribed in table 1. The roughness length for heat, z_{0h}, is prescribed as $z_{0m}/10$.

Initial soil moisture and soil temperature profiles were derived from running the control model for a single year after an initialization based on common sense. An exception is the Garderen simulation, where only 9 months of forcing data were available. There the initial soil moisture was set at field capacity (Tiktak and Bouten, 1994), while initial soil temperatures were uniformly set at the late winter climatology. Table 5 lists the selected surface characteristics and initial prognostic values. All simulations were run with a time step of 1800 s, and lasted between 9 months and nearly 3 years. Model output consisted of surface fluxes (including the separate contributions from each tile), all contributions to the tendencies of prognostic

variables, and the evolution of the soil temperature, moisture and ice content, snow depth, interception, runoff and albedo. In general, time series will be shown as 10-day averages, while monthly averaged diurnal cycles are also available. Fluxes are defined positive downward.

3 Data description

3.1 Boreas

Forcing data for the years 1994-1996 were taken from the so-called BOREAS MESONET observation network (Shewchuk, 1998) for two BOREAS Northern Study Area (NSA) sites (#8, near Thompson, Manitoba, at 55.80°N, -97.87°W, 221 m above sea level, mixed spruce and poplar with a thick moss understory and #9, 54.67°N, -101.69°W, 305 m above sea level, old jack pine in sandy soil with thin lichen surface). Observation height at both sites was 18 m, 5 m above the canopy top. Data from these sites were quality-checked, averaged and missing data were interpolated, if necessary. If possible, downward longwave radiation was derived from a radiation balance equation using observed net radiation and skin temperature. Interpolation of long gaps of shortwave and longwave radiation was carried out by scaling the diurnal cycles prior to and following the gap. Temperature above the canopy was corrected for the 80 m difference in terrain height by adjusting both temperatures with a constant value, prior to averaging. The constant was equal to plus or minus 0.5 times the average difference between the two temperature records, calculated using the entire dataset. Missing data were interpolated similarly to the radiative forcing. Wind speed was averaged per direction U and V separately.

The precipitation forcing was aggregated from a combination of the MESONET data, up to 10 rain gauges located between the #9 and the Fen site in the Sapochi river basin (data collected by R.D. Soulis, see Sellers *et al.*, 1998), and the validation data set (site TF-3, 55.879°N, -98.484°W, elevation 260 m, Northern Old Black Spruce, see below). A weighted averaging procedure was applied by number of used rain gauges as reported. Precipitation on sites #8 and #9 was taken from Belfort weighing gauges when snow depth exceeded 0, and from the tipping bucket gauges otherwise. Tipping bucket on site #8 in 1996 appeared unreliable and was discarded. The Belfort gauges can give (small) negative increments. These were compensated using adjacent time slots. Time slots with no data at all were filled with zero precipitation.

Observations of sensible heat, latent heat, friction velocity and net radiation were observed at the TF-3 old black spruce site (Goulden *et al.*, 1998). This site is already explored during the analysis of Betts *et al.* (1998b), and consists of old black Spruce, the dominant vegetation type. Additional validation data were snow depth and skin temperature measurements at the MESONET sites. Water equivalent snow depth was calculated from observed snow pack height observations by adopting the snow density formulation by Douville *et al.* (1995).

All data are available as half-hourly values between 18 Jan 1994 and 30 Nov 1996.

3.2 Mobilhy

The Hydrology - Atmosphere Pilot EXperiment (HAPEX) Mobilhy dataset (located at 43.68°N, −0.1°E) was originally prepared for a parallel simulation of multiple land surface schemes with

Table 5: Surface characteristics and initial prognostic quantities for each of the simulations. Both the control and new model parameters are shown. T_k and ω_k are soil temperature and moisture content in layer k, respectively. Interception layer was initialized at zero depth. α_n denotes background albedo in month n. Initial snow density is set at 100 kg/m^3, and initial snow albedo at 0.85. Snow temperature T_{SN} is initialized at 273.1 K. VT_H and VT_L are vegetation type indices corresponding to table 1. z is the observation height above the displacement level. $1-c_B$ is the effective vegetation fraction, calculated from the vegetation coverage attributed to the vegetation types according to table 1.

Parameter	units	BOREAS	Mobilhy	Cabauw	Garderen	FIFE	SEBEX	ARME
Similar for both models								
start date	yymmdd	940118	860101	870101	890401	870501	890719	830901
end date	yymmdd	961130	861231	871231	891231	891108	901001	851001
latitude	°N	55.879	43.683	51.97	52.25	39.029	13.25	-3.089
longitude	°E	-98.484	-0.1	4.93	5.683	-96.67	2.28	-60.187
z	m	9.33	2	20	18	2	12	18
z_{0m}	m	1.241	0.609	0.284	0.189	0.102	0.297	1.730
z_{0h}	m	0.124	0.061	0.028	0.019	0.010	0.030	0.173
T_{sk}	K	259.5	278.4	281.3	278.4	295.4	295.6	297.9
T_1	K	259.4	283.7	281.3	278.4	293.1	297.9	297.1
T_2	K	258.3	282.6	281.2	278.4	287.8	301.4	296.7
T_3	K	258.0	280.7	280.9	278.4	282.7	303.8	298.2
T_4	K	271.5	283.6	280.3	278.4	279.2	304.1	298.8
ω_1	m^3/m^3	0.250	0.318	0.316	0.323	0.217	0.258	0.307
ω_2	m^3/m^3	0.251	0.320	0.318	0.323	0.222	0.227	0.308
ω_3	m^3/m^3	0.252	0.323	0.318	0.323	0.246	0.195	0.300
ω_4	m^3/m^3	0.255	0.310	0.320	0.323	0.268	0.236	0.313
S_N	m water equiv	0.075	0	0	0	0	0	0
Control model								
α	-	0.11	0.158	0.183	0.183	0.168	0.191	0.129
c_{veg}	-	0.85	0.862	0.875	0.892	0.869	0.919	0.945
Tile model								
α_1	-	0.137	0.181	0.192	0.193	0.193	0.236	0.136
α_2	-	0.133	0.169	0.178	0.177	0.181	0.242	0.135
α_3	-	0.129	0.162	0.169	0.168	0.171	0.245	0.134
α_4	-	0.126	0.155	0.162	0.161	0.158	0.248	0.134
α_5	-	0.123	0.149	0.154	0.153	0.148	0.248	0.135
α_6	-	0.122	0.147	0.152	0.151	0.142	0.233	0.136
α_7	-	0.122	0.148	0.152	0.153	0.140	0.207	0.134
α_8	-	0.123	0.151	0.158	0.158	0.151	0.183	0.133
α_9	-	0.126	0.164	0.168	0.168	0.165	0.175	0.132
α_{10}	-	0.129	0.180	0.184	0.182	0.177	0.184	0.135
α_{11}	-	0.135	0.192	0.197	0.198	0.189	0.204	0.136
α_{12}	-	0.138	0.189	0.197	0.197	0.196	0.224	0.136
A_H	-	0.992	0.780	0.384	0.228	0.113	0.449	0.916
A_L	-	0.008	0.220	0.616	0.772	0.887	0.537	0.084
VT_H	-	3	19	19	19	19	19	6
VT_L	-	17	1	1	1	7	7	2
$1-c_B$	-	0.90	0.90	0.90	0.90	0.72	0.78	0.98

a focus on soil hydrological processes in the context of one of the PILPS activities (Shao *et al.*, 1994). The forcing and validation data were taken at the Caumont soybean field in the so-called SAMER flux station network (Goutorbe, 1991). The vegetation on that site showed a significant development during the season. The soil was practically bare before May and after harvest in September, while in the intermediate growing season the crop emerged and formed a dense ($LAI = 3$) canopy. Coniferous forest and crops form the two main vegetation types in the surrounding area.

Surface energy fluxes were only measured in a limited period (28 May - 3 July 1986; see Mahfouf, 1990). During this period, latent heat flux was not measured directly, but obtained as a residual from the energy balance equation. Soil moisture measurements were carried out roughly weekly in a profile extending to 1.6 m depth. A Penman-Monteith estimate of the evaporation loss throughout the year was calculated from the observations of precipitation and soil moisture change by Mahfouf (pers.comm.).

3.3 Cabauw

The Cabauw-1987 dataset (51.97°N, 4.93°E) was prepared by Beljaars and Bosveld (1997) for the PILPS intercomparison study reported by Chen *et al.* (1997). Observations are taken at a grassland-site near the 200 m meteorological observation tower. Surface sensible heat flux is obtained from the profile method, and latent heat is calculated as a residual of the surface energy balance. Extensive data quality checking and gap interpolation have been performed by Beljaars and Bosveld (1997).

Data from this site are collected in a nearly continuous monitoring program. They have for instance been used for studies focusing on evaporation of wet grassland (Beljaars and Viterbo, 1994), roughness length ratio (Beljaars and Holtslag, 1991) and interaction between land surface and the planetary boundary layer (Ek and Holtslag, 1999). VB95 used the same 1987 dataset for the evaluation of the previous version of the ECMWF surface scheme.

3.4 Garderen

The Garderen site is a dense Douglas fir forest location in the Speulderbos, in the centre of the Netherlands (52.25°N, 5.68°E; Bosveld, 1997). A continuous record of quality-checked and gap-filled meteorological data was available for 9 months in 1989. Data were collected at a 36 m tower in the centre of a patch of moderately homogeneous forest. Wind direction determined the length of homogeneous fetch, and was used to cancel out unrepresentative flux measurements. Roughness length and dispacement height are found to be slightly wind speed dependent. Leaf area of the stand varied somewhat throughout the year, but on the average was very high ($LAI \approx 10\ m^2/m^2$).

Flux measurements were carried out using eddy-correlation equipment. This yielded a nearly continuous record of sensible heat flux, but latent heat flux eddy-correlation data are often missing due to equipment failure. A continuous record of latent heat flux has been constructed by filling gaps with energy balance closure residuals. Also available was an independent dataset from a set of sapflow devices (Bosveld and Bouten, 1999a). These observations were lacking during the first few weeks of the simulation period, but covered the remaining period

very well. Bosveld and Bouten (1999b) analyse the environmental controls on forest evaporation using a Penman-Monteith framework with a calibrated canopy resistance. They find a close correspondence between the (calibrated) Penman-Monteith model evaporation and the sapflow measurements. The eddy-correlation/energy balance derived time series of LE is systematically higher than the sapflow data, which is attributed to contributions of soil evaporation and evaporation from intercepted water.

3.5 Fife

The dataset from the First ISLSCP Field Experiment (FIFE) was prepared by Betts and Ball (1998). It is an extension of the dataset covering the growing season in 1987, used for validation of the previous release of the ECMWF surface scheme (VB95). Near-surface meteorological quantities and radiative forcing were aggregated from carefully cleaned measurements from 10 automatic weather stations. Large gaps occurred in the measurement record of downward longwave and shortwave radiation, in particular in the winter and spring of 1987-1988. These data were replaced by closest grid point calculations from the ECMWF ERA15 cycle. ERA15 shortwave radiation data were reduced to 92% of their original value, in order to get the closest correspondence with local FIFE measurements. ERA15 data were linearly interpolated in time, matching the original time resolution. Wind speed was observed at 5.4 m height (Betts and Ball (1998) in error reported 2 m). A neutral logarithmic profile was assumed to extrapolate observed wind speeds to 2 m height.

Gaps in the forcings were interpolated by either a linear interpolation (wind, pressure) or by a trend in the diurnal cycles (temperature). Specific humidity was calculated from an interpolated relative humidity, to avoid super-saturation.

A site-averaged surface flux dataset was constructed from available measurements during the summer months in 1987 and 1988. Eddy-correlation measurements were conducted during four intensive field campaigns in 1987 (including up to 22 surface flux stations), and outside these campaigns flux data are obtained by Bowen ratio devices. In 1989 flux measurements are available only during a short intensive observation period.

3.6 Sebex

The Sahelian Energy Balance EXperiment (SEBEX, Wallace *et al.*, 1991) is a measurement campaign that took place in 1989-1990 in the Sahelian zone of West-Africa. Its objective was to obtain surface energy balance data from three contrasting vegetation types in that area for remote sensing purposes.

For the present study, data from the fallow savannah site (at the so-called ICRISAT Sahelian centre, 13.25°N, 2.28°E) were used. At this site, occasional trees were found in a field mainly covered with low natural vegetation (80% of the area) and low shrubs (20%). At the site a thin (0.2-0.5 m very sandy soil overlying laterite was found.

Observations were made of net and shortwave radiation, sensible heat flux by means of a one-dimensional eddy-correlation device, and an automatic weather station. Soil heat flux, reflected shortwave radiation and surface temperature were measured separately for the bushes

and low vegetations. An aggregated set of forcing and validation data was provided by S. Allen (priv.comm.).

Unfortunately, sensible heat flux measurements were not available in the dry season between December 1989 and April 1990. Verhoef *et al.* (1999) estimated a daily averaged sensible heat flux from a linear regression against the difference between the surface temperature at 1400 UTC and the maximum air temperature. In combination with the (nearly) continuous record of net radiation, an estimate of the daily total evaporation loss was made. The site was also used in 1992 in the context of the HAPEX-Sahel experiment (Goutorbe *et al.*, 1994).

3.7 Arme

Shuttleworth *et al.* (1984) describe observations of forcings and energy fluxes over a representative terra firma forest site in the Brazilian part of the Amazonian tropical forest area. More than two years of hourly observations of standard meteorological and radiation forcings were collected during this ARME (Amazonian Regional Meteorological Experiment) campaign in the Ducke Reserve near Manaus (2.95°S, 59.95°W). Observations were taken at approximately 10 m above the canopy. The roughness length of the site was estimated to be 1.7 m, while z/z_{0m} was assumed to be approximately 10.4 (z being the measurement height above the displacement level), resulting in an estimated value for z of ± 18 m.

Fluxes of sensible and latent heat were measured using 1-dimensional eddy-correlation during selected time intervals. Shuttleworth (1988) analysed the data using a calibrated model describing the forest evaporation. An estimate was provided of the monthly total evaporation and interception loss. The dataset was used by VB95 for an evaluation of the previous version of the ECMWF surface scheme.

4 Results

4.1 Boreas

Figure 2 convincingly shows a significant improvement of the new model formulation for the BOREAS latent heat fluxes. The control model shows large peaks of evaporation in winter and early spring, and higher summertime evaporation. The excessive winter/spring evaporation in the control model is mainly caused by two misrepresented processes, both redesigned in the new model:

- In order to alleviate severe cold biases over boreal areas in the global simulations, Viterbo and Betts (1999) concluded that the model snow albedo for forested areas was not realistic and should be limited to 0.20. However, as long as the grid box was occupied by snow, the increase in net radiation was used to evaporate the snow, which is the dominant contribution to the total evaporation in figure 2. Thus, the reduction of the cold bias was realized by adding latent heat rather than sensible heat to the atmosphere. Indeed, precipitation was clearly overestimated for the Boreal areas (Betts and Viterbo, 2000). In the new model snow evaporation from the forest tiles is limited due to the positioning of the snow layer *under* the canopy layer (where a significant portion of radiation is

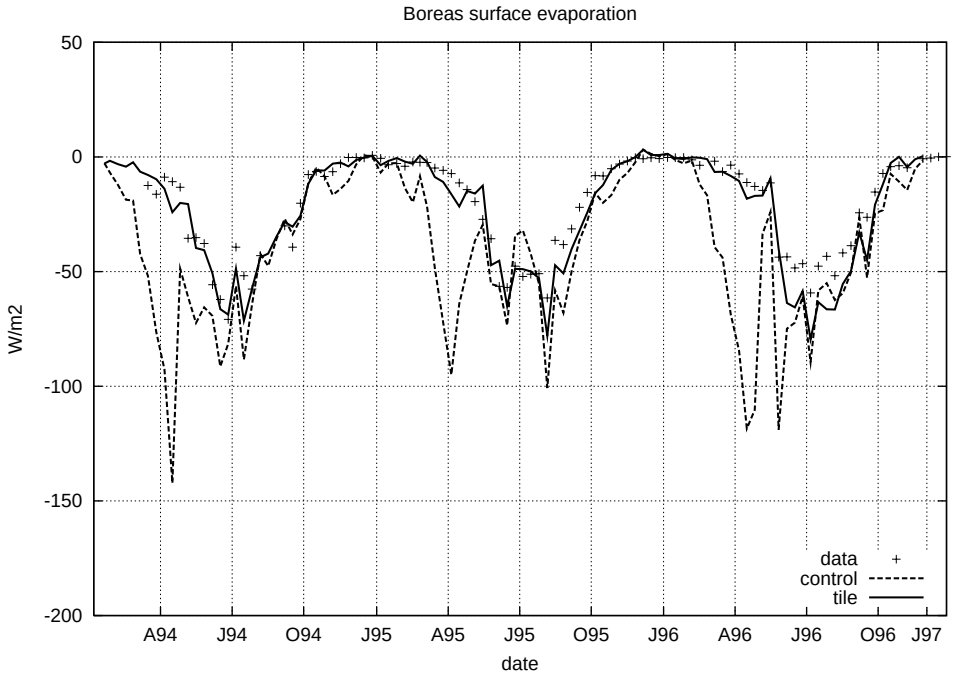

Figure 2: 10-day averages of BOREAS total evaporation from observations and simulations by the control and tile model.

intercepted and used mainly to heat the atmosphere by sensible heat release) and an extra aerodynamical resistance to the snow pack (equation 12);

- Canopy transpiration and root extraction was not limited in case of frozen soils. In particular during the Spring melt season, when snow already disappeared from significant portions of the grid box but where the underling soil is still frozen, canopy transpiration is too high. This is avoided by parameterizing the soil water stress using the liquid soil water portion only.

The impact of the reduced snow evaporation is also visible from the simulated snow depth (figure 3). The control model shows a too early disappearance of the snow pack by several weeks, while the tile model successfully allows the snow pack to build up more and reside until high enough air temperatures allow it to melt. The peak snow height is still underestimated. This might have three reasons: first, the model spreads the snow deck uniformly over the grid box, while in reality a concentration of snow on specific locations is caused by snow drift and topographic variability; second, the observed snowfall may be biased low, leading to an underestimation of the modelled snow pack increase; and third, the derivation of the water equivalent snow pack from the observations using a snow density formulation by Douville *et al.* (1995) is rather indirect. The limitation of soil infiltration while the soil is frozen (which is the case during snow melt) results in strong runoff peaks in spring (figure 4). In fact, the control model does not display any significant runoff. The tile model shows a secondary runoff period in later summer/early autumn. This deep water drainage is water that is transported "step-wise" downward through the column, trapped on top of lower frozen layers. The water

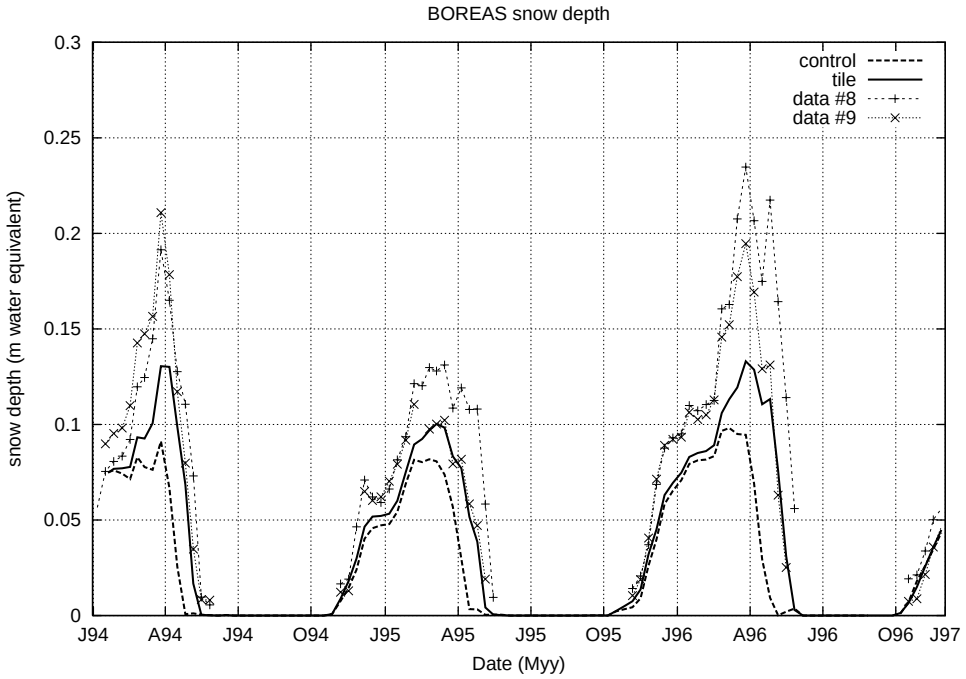

Figure 3: 10-day averages of BOREAS snow depth (in m water equivalent) as observed at MESONET sites # 8 and #9, and modelled by the control and modified scheme. Observed snow pack height was converted to water units adopting the snow density formulation by Douville *et al.* (1995).

is only released from the model soil volume after the lowest soil layer becomes unfrozen.

A marked change is visible also in the simulated near-surface soil temperature (Figure 5). The control model calculates much colder near-surface soil temperatures owing to a lack of insulation by a snow deck on top of the soil, which is present in the new tiled scheme. The tiled model with insulating snow follows the annual cycle of the soil temperature at the upland feather moss site, while the soil barely freezes under the low lying spagnum moss layer owing to the additional insulating properties of the moss. In summer the two models show similar behavior.

Another feature introduced in the new surface scheme affecting the surface energy balance of forest is the asymmetric skin conductivity, being larger during unstable forest conditions (usually during nighttime) than during stable stratification (table 2). Figure 6 shows an averaged diurnal cycle of total sensible heat flux for April 1996, where snow still occupies the largest portion of the gridbox. As well as the large difference in daytime sensible heat transfer related to the reduction of the snow evaporation described above, the nighttime heat flux is now upward throughout the night. The skin temperature (which is the forest canopy temperature) is linked more strongly to the cooler underlying snow than in the control model, and this gives better agreement with the observed heat fluxes.

Figure 7 shows the daytime evaporative fraction for July 1996. Observations show very little change of the evaporative fraction during the day (Betts *et al.*, 1999). In the control model, the lack of stomatal control causes an increase of the afternoon evaporative fraction, which is reduced in the tile model by incorporating the vapour pressure stress function (equation 10).

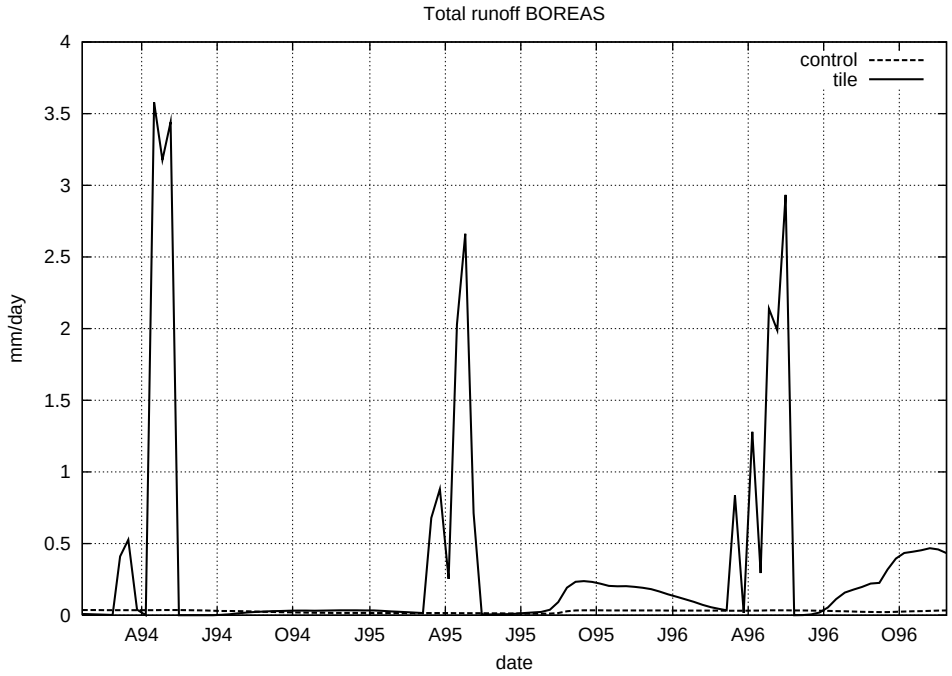

Figure 4: 10-day averages of simulated BOREAS total runoff, for both the control and tile model.

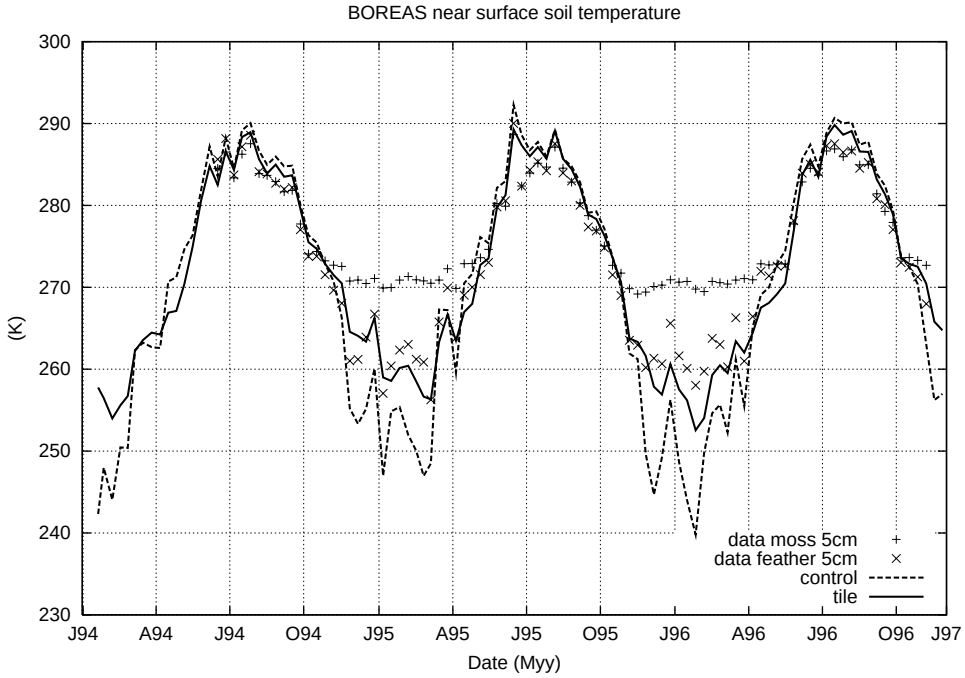

Figure 5: Soil temperature measured at 5 *cm* deep for the moss and feather understories, and simulations of the upper soil layer of 7 *cm* depth by the control and new scheme.

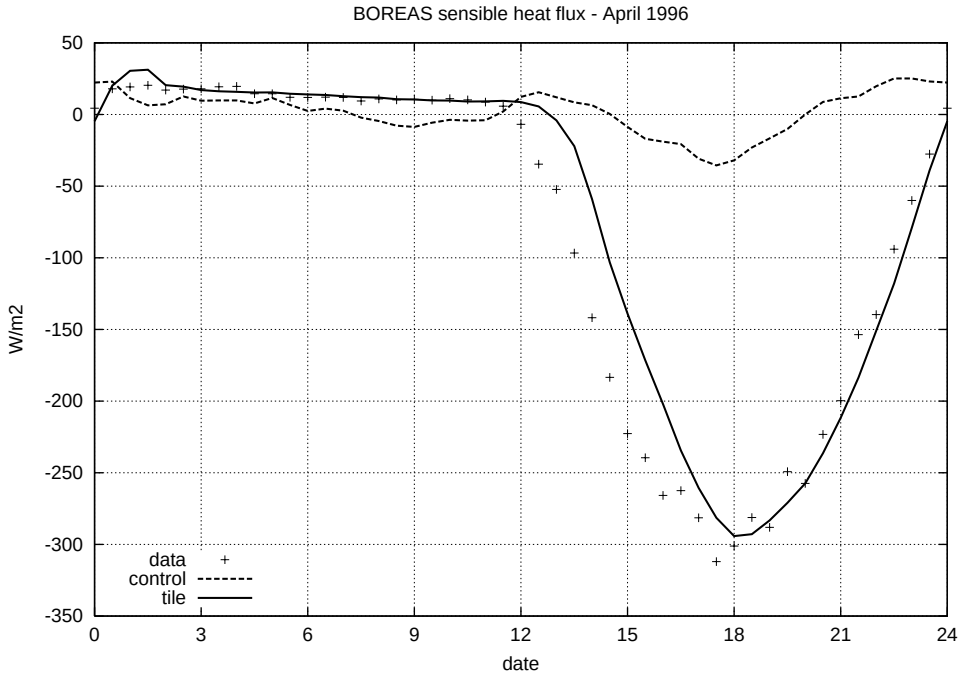

Figure 6: Averaged diurnal cycle of sensible heat flux for the BOREAS case in April 1996, for the observations and the control and tile model.

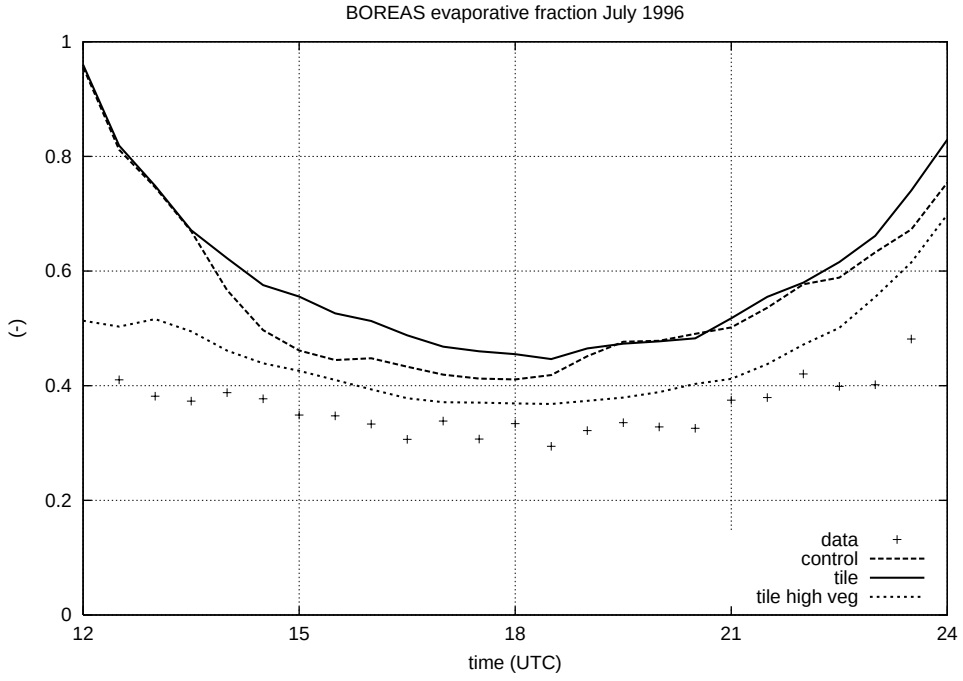

Figure 7: Averaged diurnal cycle of evaporative fraction for the BOREAS case in July 1996, for the observations and the control and tile model. Tile model results are shown for the grid box total flux partitioning and from the high vegetation tile separately.

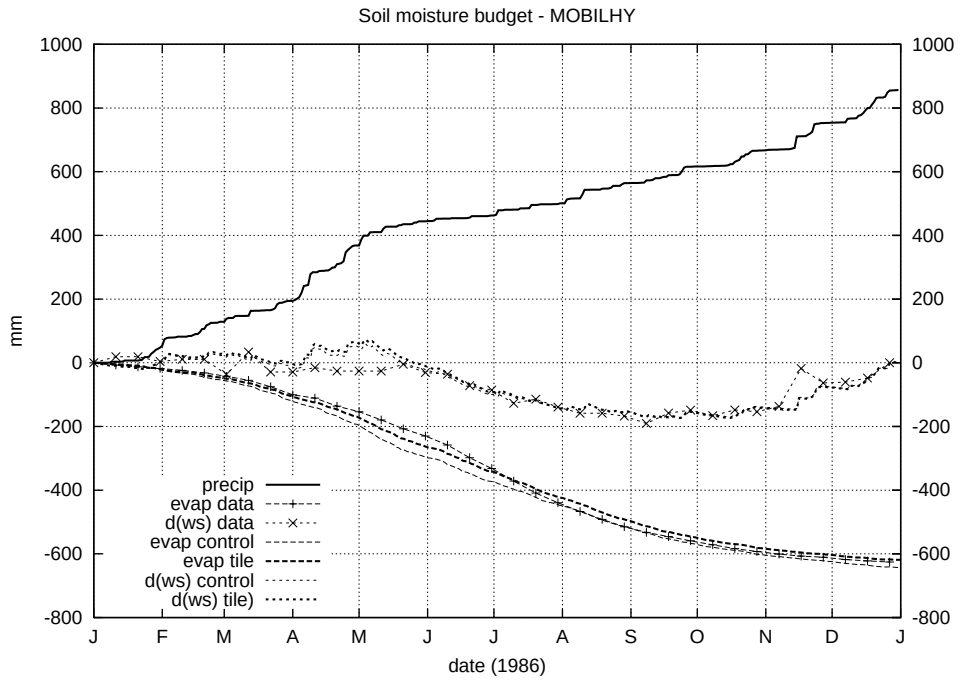

Figure 8: Cumulative soil hydrological budget for the HAPEX- Mobilhy site. Shown are observed precipitation (upper line), change of the soil water reservoir in the total observed 1.6 m deep column (central line), and evaporation from a calibrated Penman-Monteith model (bottom line). Simulations of both the control and the tile model are included.

The diurnal course of the forest tile now compares better with the observations at the black spruce site. The relatively large difference between the modelled evaporative fraction from the forest tile and the total grid box is mainly caused by the high evaporation rates from the interception tile, which significantly contribute to the total grid box evaporation.

4.2 Mobilhy

The model changes particularly relevant for the HAPEX-Mobilhy site concern:

- a change of the vegetation structure: the tile model assigns the site of HAPEX-Mobilhy to be dominantly covered with interrupted forest, while less than 25% is occupied by crops. In the control model we have 86% of "crop-like" vegetation (see table 5).

- a change of the bare soil evaporation formulation, replacing the relative humidity approach by a resistance approach.

In figure 8 the cumulative soil water budget (without the runoff term) is shown, as derived from the observations and calculated by the control and tile model. Despite the significant difference in structure, canopy resistance parameterization and root extraction of the models, the cumulative evaporation and soil water storage are very similar. In the tile model the high vegetation tile gives lower transpiration rates then the vegetation in the control scheme, but

Table 6: Cumulative evaporation (mm) for the HAPEX-Mobilhy site from the bare ground, vegetation and interception components. Canopy evaporation from the tile model is a summation of the high and low vegetation tiles. Accumulation is over the entire simulation period.

Model	**bare ground**	**canopy**	**interception**	**total**
control	62	428	148	638
tile	83	406	129	618
estimated				627

the low vegetation transpiration compensates this, presumably by a combined effect of deeper roots and slightly higher skin temperatures.

Early in the season the models show a small overestimation of evaporation, but this is compensated later on, to end with very similar results. The good correspondence to the observations (a calibrated Penman-Monteith estimate) shows the dominating role of available energy in the determination of surface evaporation.

However, the partitioning of the evaporation over the various grid box elements is changed considerably. Table 6 shows the accumulated evaporation loss from the vegetation, bare ground and interception reservoir. The total evaporation from the tile model is 20 mm less than the control. The effective leaf area index ($c_{veg} \times LAI$) is reduced by 30% from 3.45 in the control to 2.35 in the tile scheme, but the associated reduction in canopy and interception evaporation is partially compensated by an enhanced bare ground evaporation. Since bare ground dominated the site before May, the improved correspondence between the tile model and the calibrated site estimation might be attributed by an increased role of bare ground evaporation from the tile scheme.

The difference in observed and simulated soil moisture change suggest the models may underestimate deep water drainage early in the season. Integrated over the year the soil water budgets of both schemes match estimations based on data rather well.

4.3 Cabauw

As HAPEX-Mobilhy, the changes to the ECMWF surface scheme relevant to the Cabauw site are a changed characterization of the surface parameters. The grid-box averaged latent heat fluxes for the Cabauw-1987 case are however rather similar for both model versions (see figure 9). The winter evaporation is slightly reduced in the tile model, owing to a smaller leaf area index (both from the low and the high vegetation tile) and an associated reduction in interception evaporation. In the tile model, however, there are large differences between the evaporation from the high vegetation (interrupted forest) and low vegetation (cropland). In winter, evaporation from the high vegetation is comparable to the crop transpiration, but in summer the stronger stomatal control of the high vegetation results in ± 20 W/m^2 lower transpiration rates (figures not shown). The tile model shows a slightly larger seasonal cycle in total evaporation, but in both model versions this is less pronounced than the observations. The lack of a seasonal cycle in leaf area index results in overestimated evaporation from the interception reservoir in winter, and an underestimated canopy transpiration in summer, which partly compensates for

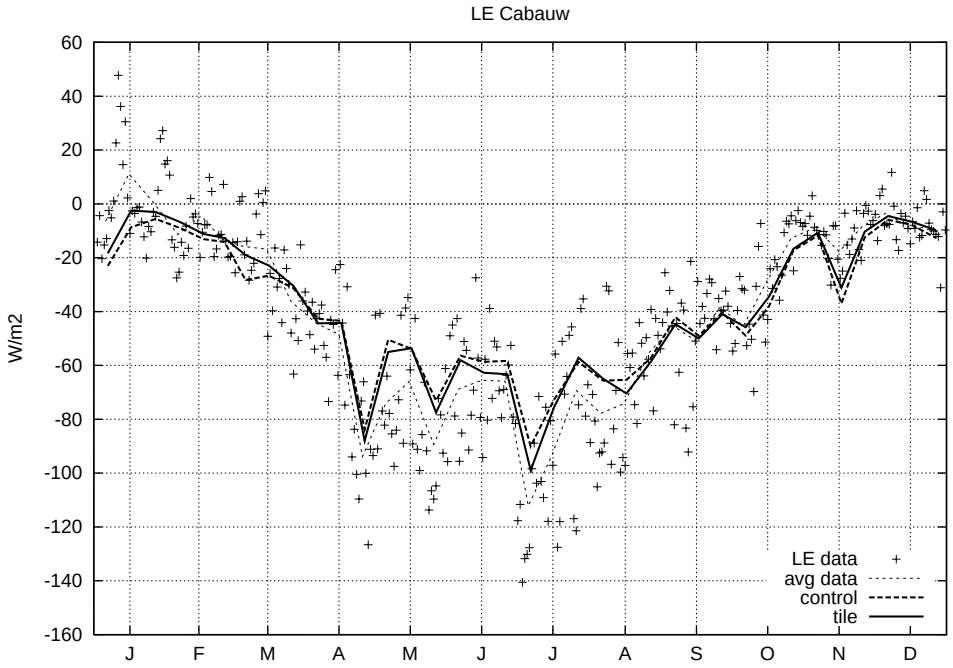

Figure 9: Averaged latent heat flux from the Cabauw site. Shown are daily (symbols) and 10-day (thin lines) averaged data, and 10-day averages of the control and the tile model.

the excess winter evaporation.

The diurnal cycle of the skin temperature in summer (figure 10) is not changed much. Both the control and the tile model show good agreement of nighttime skin temperature with data, and an underestimation and lag of the daytime temperature maximum. This is apparent in both wintertime and summertime conditions. The tile model has a slightly larger diurnal cycle than the control.

The direct transmission of shortwave radiation to the top soil layer (equation 1) has a clear impact on the average soil temperature. The entire soil column is warmed approximately 1 K (figure not shown).

4.4 Garderen

The Garderen data are collected over a dense Douglas fir stand, while the tile model assumes less than 25% to be occupied by interrupted forest, the rest being cropland. Indeed, the site is very close to the Cabauw site discussed before, and has a similar climatology. Since the atmospheric forcing and the observations were representative for the forest stand, we will focus at the model results with some relevance to the high vegetation representation in the scheme, namely, the canopy resistance and the asymmetric value of Λ_{sk}.

Figure 11 shows 10-day averaged total surface evaporation during the simulation period, both observed and modelled. The observations contain some uncertainty, as is clear from the difference between the time series obtained by eddy-correlation with gaps filled in by energy balance closure terms on one hand, and sapflow observations on the other. A systematically

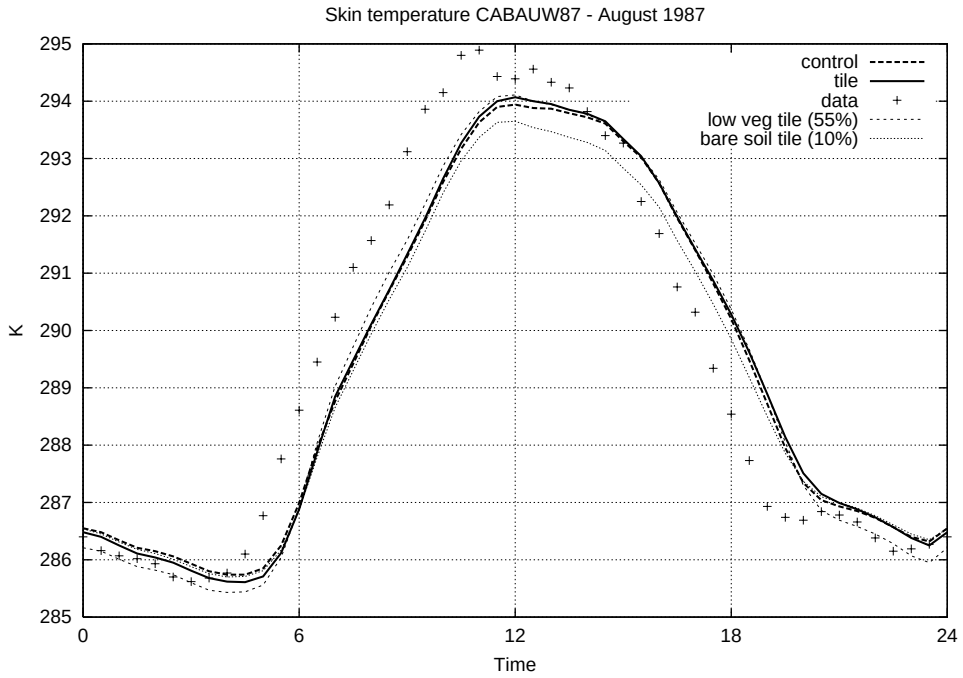

Figure 10: Averaged diurnal cycle of observed and modelled skin temperature for August 1987. Shown are data derived from observed upward longwave radiation, and skin temperatures from the control and tile model. From the tile model, skin temperatures from the low vegetation and bare soil component are shown as well.

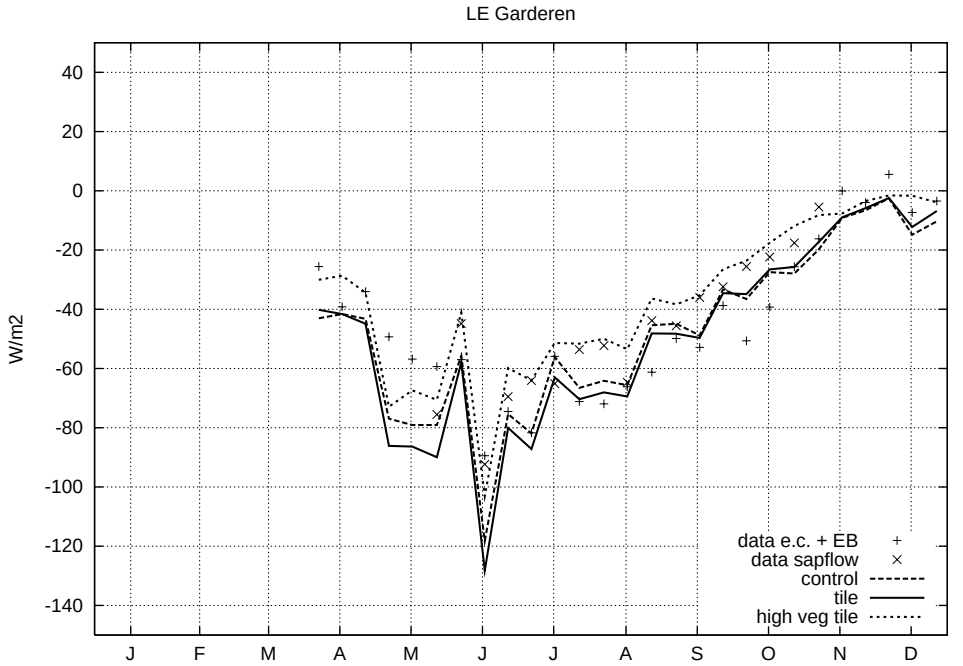

Figure 11: Observed and simulated total surface evaporation for the Garderen case. Shown are observations of eddy-correlation combined with energy balance residuals as well as sapflow data. Model simulations shown include total evaporation by the control and the tile model, as well as output from the high vegetation tile.

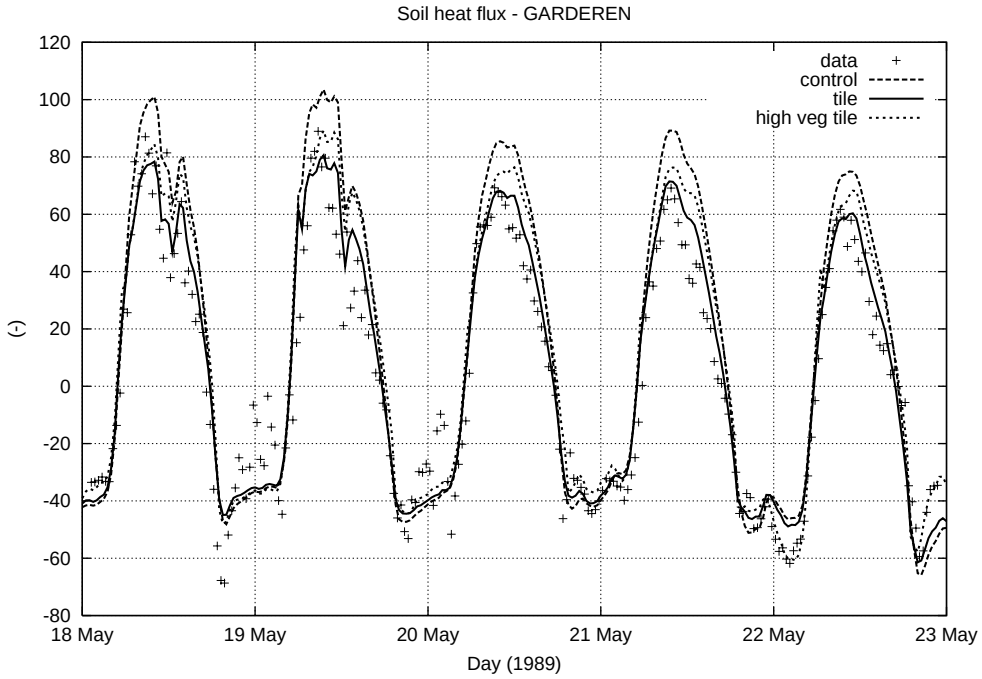

Figure 12: Observed and simulated soil heat flux for a series of days in May 1989. Shown are observations of the storage heat flux, and simulations of $\Lambda_{sk}(T_{sk} - T_1)$ for both the control and the tile model. Also shown is this quantity for the forest tile in the tile scheme.

lower evaporation from the sapflow record may be expected as evaporation from soil and intercepted water is not included. The difference is typically 15 W/m^2, which is about 30% of the annual mean evaporation. Tiktak and Bouten (1994) report interception losses as high as 38% for this forest site, and attribute the high value to the density of the stand ($LAI = 10$).

Both the control and tile model show an overestimation of evaporation in the first three months of the simulation, followed by a simulated evaporation that is too low later in the year, when compared with the eddy correlation/energy balance observation record. This is consistent with the findings of Bosveld and Bouten (1999b), who show that the transpiration response to soil water potential is different for the periods before and after 23 July 1989. A canopy resistance model calibrated on available flux and soil moisture data explained much more of the variance when soil water stress was ignored after this date. They explain this from a dynamic adjustment of the canopy root system to the dry summer conditions. A comparison between calculated evaporation from the high vegetation tile to sapflow data confirm that the simulated transpiration levels are generally lower than observed. Unfortunately, no sapflow data are available during the first months of the simulation period.

The surface characteristics of the high vegetation tile (in particular albedo and roughness length) which were specified from the climate database, differ greatly from the local conditions. A sensitivity experiment was carried out in which these characteristics (surface albedo, aerodynamic and heat roughness) were derived from observations by Bosveld (1997). The whole gridbox was covered with evergreen needleleaf forest. This simulation showed that the total gridbox evaporation went up by typically 35% compared to the output from the high vegetation

tile in the previous simulation. However, the evaporation from the high vegetation tile did not change very much in spite of the change in albedo and roughness. The grid box evaporation changed mainly by an increased interception loss. The canopy transpiration is rather insensitive to the prescribed albedo and roughness, but more so to the high value of the canopy resistance.

Another interesting feature highlighted by Bosveld *et al.* (1999) is the asymetric coupling of the forest interior to the overlying atmosphere. In the tile model this is included by using a different value of Λ_{sk} for stable and unstable conditions. Figure 12 shows a time series of the observed storage heat flux and the simulated soil heat flux (excluding the direct radiative transfer, $f_{Rs}(1-\alpha)R_s$) for a series of days in May 1989. The nights of 18-19 May were mentioned by Bosveld *et al.* (1999) as an example of a decoupled forest interior owing to low wind speeds, whereas during the night of 21-22 May strong winds caused a close correspondence between the temperatures of the canopy and the forcing air. A strong cooling of the forcing temperature on 21-22 May, which brings the canopy (skin) temperature down as well, is immediately felt in the nighttime soil heat flux from the forest tile, in agreement with observations. This is not so in the control model and the grid box average tile model (which is dominated by low vegetation with a symmetric Λ_{sk}).

4.5 Fife

VB95 used the FIFE 1987 flux dataset for an evaluation of the control scheme. On the average, the evaporation in their model appeared too low, in particular during the dry periods in summer. They concluded that the correspondence between model and data was better during the intensive observation periods, when eddy correlation data were included, than during the periods in between these, where Bowen ratio equipment was used to determine surface fluxes. In contrast, Betts *et al.* (1998c) found a fair agreement between observed surface turbulent fluxes and simulations done in the first ECMWF Reanalysis. They conclude that soil moisture nudging (Viterbo and Courtier, 1995) in ERA15, being an additional net source of soil water, may at least partially be responsible for an increase in surface evaporation.

In the tile scheme the FIFE site is represented by mainly tall grass, which has a deeper rooting and lower $r_{s,min}/LAI$ than the control, but also a larger fraction of bare soil (see tables 1 and 5). The new scheme produces a cumulative evaporation over the whole period 1987-1989 which is 5% higher than the control model, as the changed canopy properties and decreased vegetation coverage for the tall grass vegetation type have impacts that partly compensate. Figure 13 compares daily averaged surface evaporation in 1987 from both model versions with data, as well as the accumulated evaporation loss. It is during the growing season that the tile model shows an enhanced evaporation. In addition, the deeper root profile helps sustain surface evaporation during the dry spell in late July 1987.

The underestimation of evaporation is still considerable. At least three causes for this may be identified. First, the canopy resistance coefficients for the vegetation types involved can be wrong. Choices of these are necessarily a compromise because there is significant variability with season and location. For instance, the tall grass vegetation type, dominant for the FIFE area, is relatively sparse on the American continent, but much more widespread in the Sahel area (see the SEBEX simulations below). Both areas have strong seasonal cycles which are not represented in the current model. In addition, the low surface evaporation is a weighted

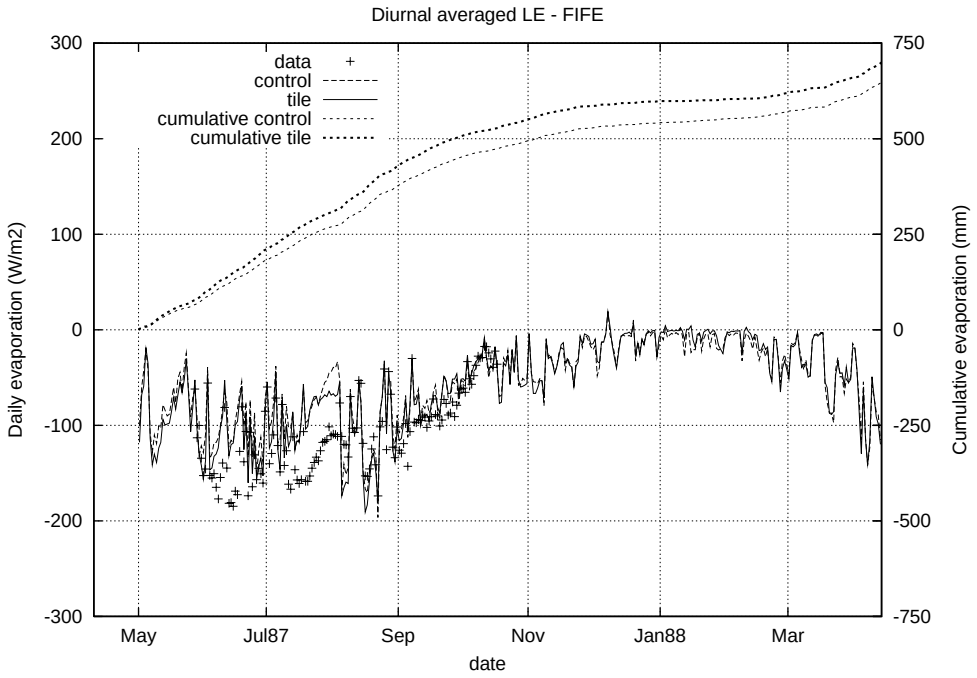

Figure 13: Comparison of total surface evaporation by the control and the tile model to 1987 FIFE observations (left axis), and cumulative evaporation losses for both model simulations (right axis).

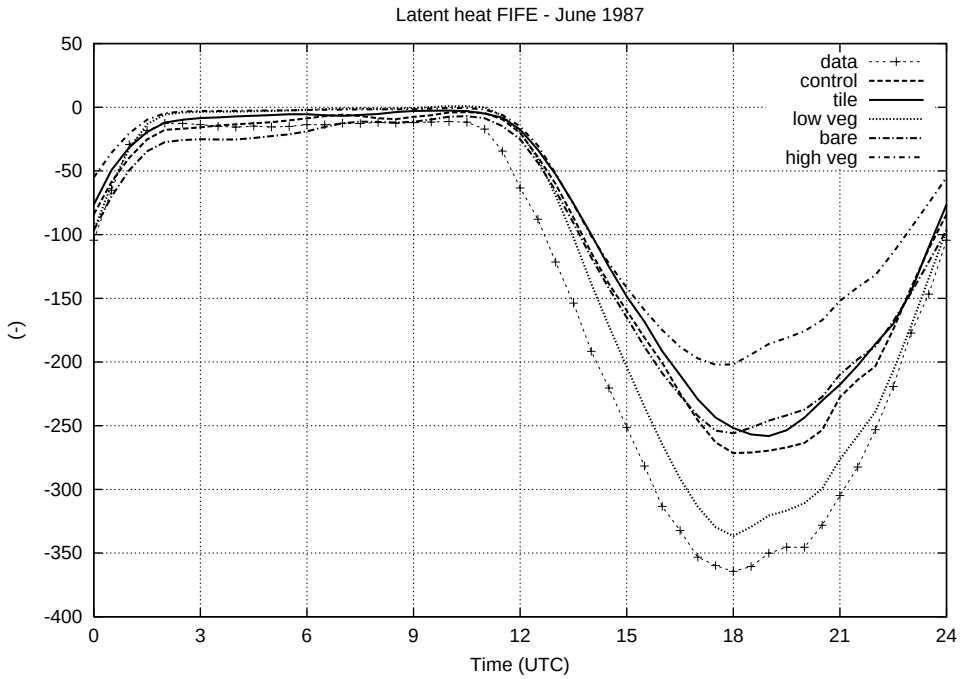

Figure 14: Average diurnal cycle of latent heat flux for the FIFE site in June 1987, for observations and various model simulations.

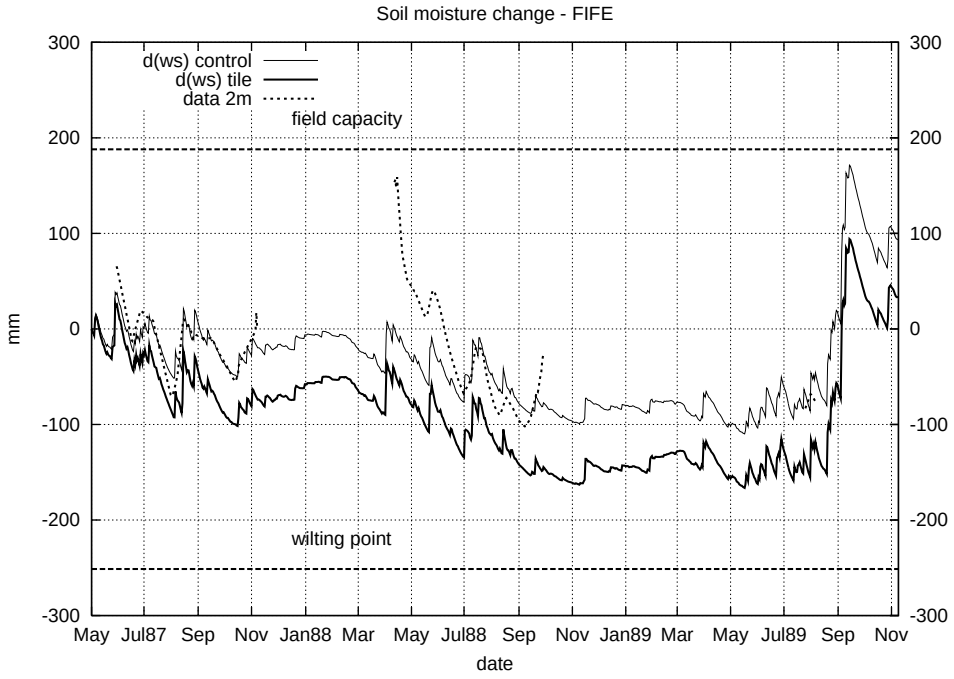

Figure 15: Cumulative FIFE moisture change in the total soil volume relative to the initial profile, for both the control and tile model.

average of the various tiles in the gridbox. Figure 14 shows the average June 1987 diurnal cycle for the evaporation, from data, the control model and various tiles in the tile model. The tall grass tile (low vegetation type), which covers only 62% of the grid area in the model, shows a better correspondence to data (collected primarily over grass sites) than the average evaporation, indicating the sensitivity of a mismatch of the coverage coefficients.

Second, the ERA15 shortwave radiation appears approximately 8% higher than the aggregated data from Betts and Ball (1998). Indeed, simulated net radiation in the offline experiments is lower than observed, resulting in a reduction of surface turbulent fluxes (figures not shown).

Third, there is severe soil moisture stress encountered during the growing season in both the control and tile model. Figure 15 shows the change of soil water in the total 2.89 m soil column relative to the initial profile, having an average volumetric water content of approximately 0.258 m^3/m^3. Also shown are the levels of the model field capacity and wilting point. The initial profile is obtained from a one-year integration of the control model, initialized at field capacity (0.323 m^3/m^3). Initializing both schemes at field capacity would increase the surface evaporation only during the first couple of weeks of the simulation, since at high water levels the soil scheme has rapid base drainage. Figure 15 clearly shows that the water level in the soil is well below field capacity during nearly the entire period, resulting in a considerable soil moisture stress to canopy transpiration.

Figure 15 also shows the change of observed soil water content of a 2 m deep profile, referenced arbitrarily to the model's field capacity, which is not necessarily correct for this actual location. Nonetheless, the data make clear that the low frequency variation of the observed

total soil water content is considerably larger than either the control or the tile model. It is likely that root extraction (and thus surface evaporation) is indeed underestimated by both schemes.

Figure 15 also makes clear that the higher evaporation from the tile model results in a lower equilibrium soil water content than the control scheme. The negative feedback of root stress will eventually shut down the excess surface evaporation introduced by the reduction of $r_{s,min}/LAI$ in the tile scheme compared to the control. On a seasonal time scale, higher evaporation amounts thus have to be realized by a reduction of the water loss through drainage or surface runoff. These soil physical characteristics were not changed in the tile model, which is a likely reason for the limited impact of the adjustments of the surface canopy characteristics.

Simulated soil temperatures are higher in the tile scheme, and more in agreement with data than the control model (see figure 16). Both models simulate too low a temperature in the 1987-1988 winter, but at both levels shown the tile model is somewhat better during the other seasons. Both the modified soil thermal coefficients and the direct absorption of shortwave radiation by the upper soil layer are responsible for this improvement.

4.6 Sebex

The SEBEX dataset is characterized by a pronounced seasonal hydrological cycle. A dry season without precipitation and with low evaporation starts in the middle of November 1989, lasting until May 1990. Unfortunately, direct observations of surface evaporation are available in the dry seasons only, and the best possible estimate of water loss in the dry season is provided by the estimation of Verhoef *et al.* (1999).

The most significant differences between the control and tile model for the SEBEX simulation are

- a decrease of the minimum canopy resistance from $r_{s,min}/LAI = 272/4$ (See footnote of table 1) to 80/2 for the tall grass tile;
- a decrease of the gridbox fraction covered by vegetation (from 0.92 to 0.78; see table 5);
- a change of the root extraction profile, yielding more extraction from the top and second layer and some extraction from the deepest one, at the cost of the third layer (see table 3);
- A change of the bare soil evaporation from a relative humidity formulation to a resistance approach. This basically implied that bare ground evaporation is now shut of when the moisture content in the upper soil layer reaches wilting point, whereas in the control model it continued to drier moisture levels; and
- an change in the surface albedo from a constant 0.19 to a seasonal cycle, ranging between 0.17 and 0.25.

Differences between simulations of the control and tile model are most pronounced in the dry season. Once the rains stop, the control model responds quickly with reduced evaporation. In the dry season, bare soil evaporation is the main source of water (see figure 17). The tile

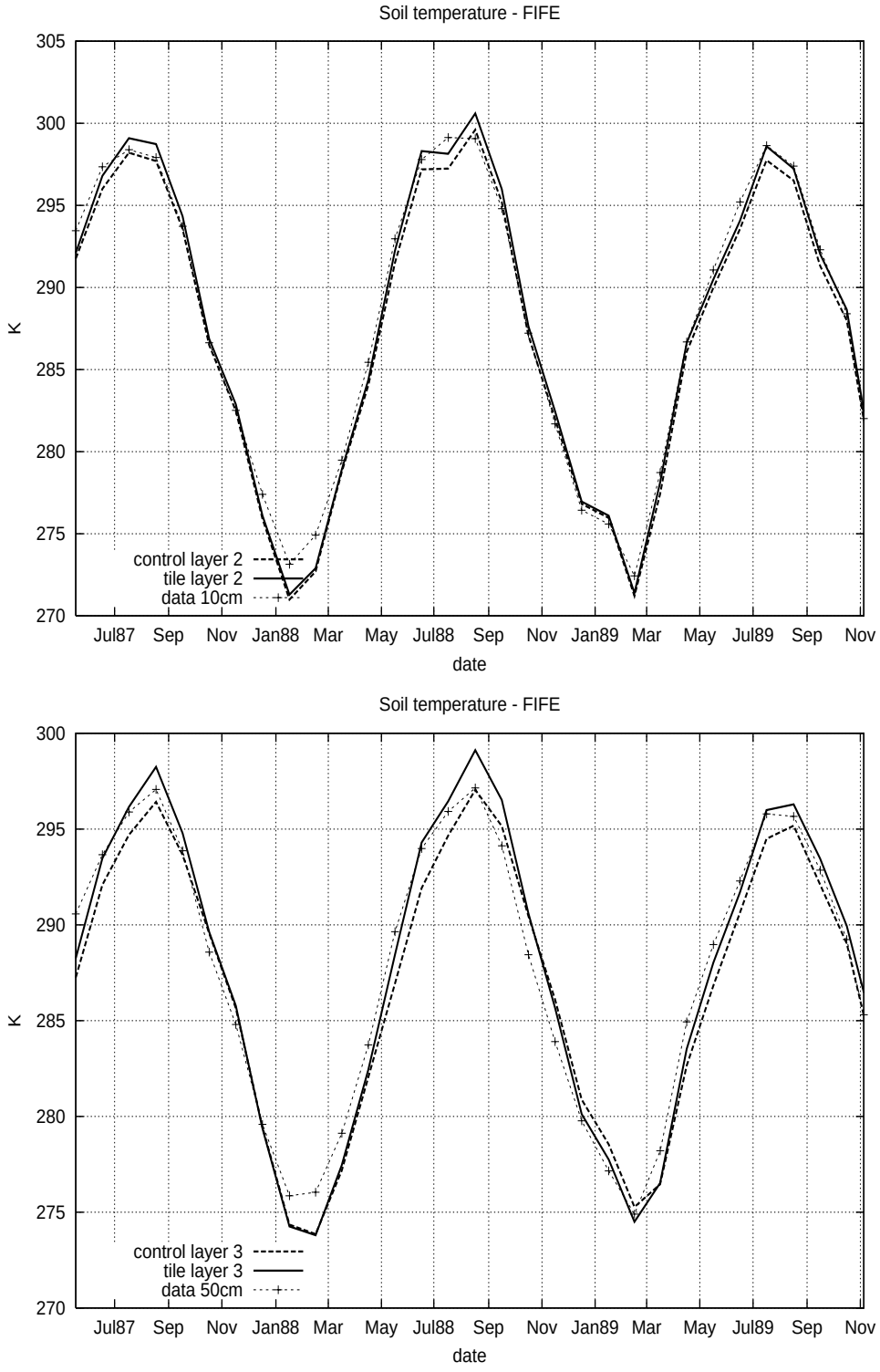

Figure 16: Soil temperatures observed during FIFE at depths of 10 *cm* (upper panel) and 50 *cm* (lower panel), plotted together with model simulations in layers 2 (7 - 28 *cm*, upper panel) and 3 (28 - 100 *cm*, lower panel). Upper panel data and model output is averaged over 10 day intervals, and the lower panel shows daily averages.

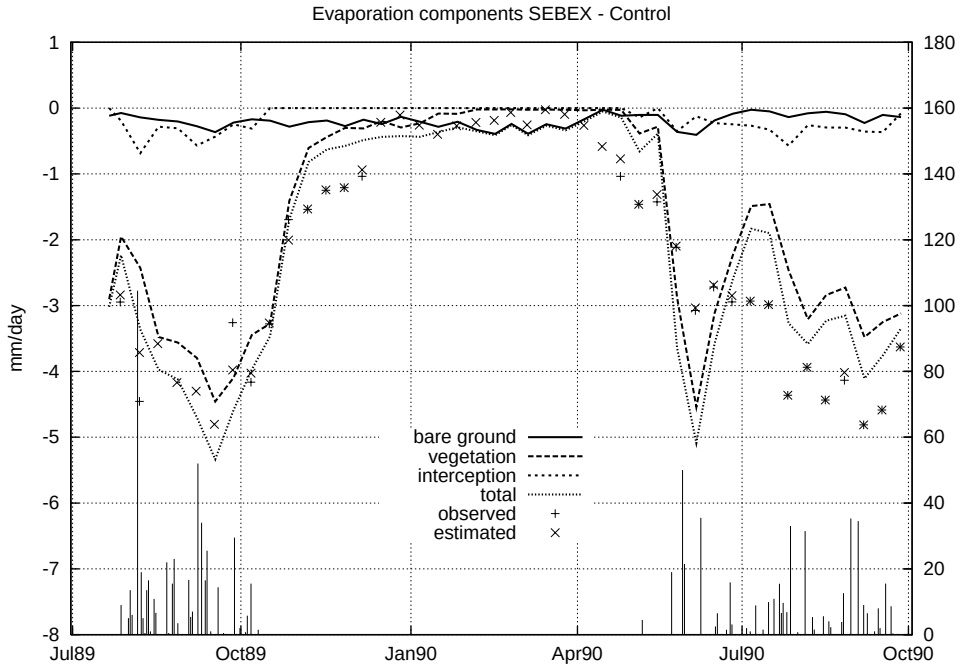

Figure 17: Simulated evaporation, distinguished between canopy transpiration and evaporation from bare soil and interception reservoir, for the control model. Also shown are measured and estimated evaporation rates and daily precipitation.

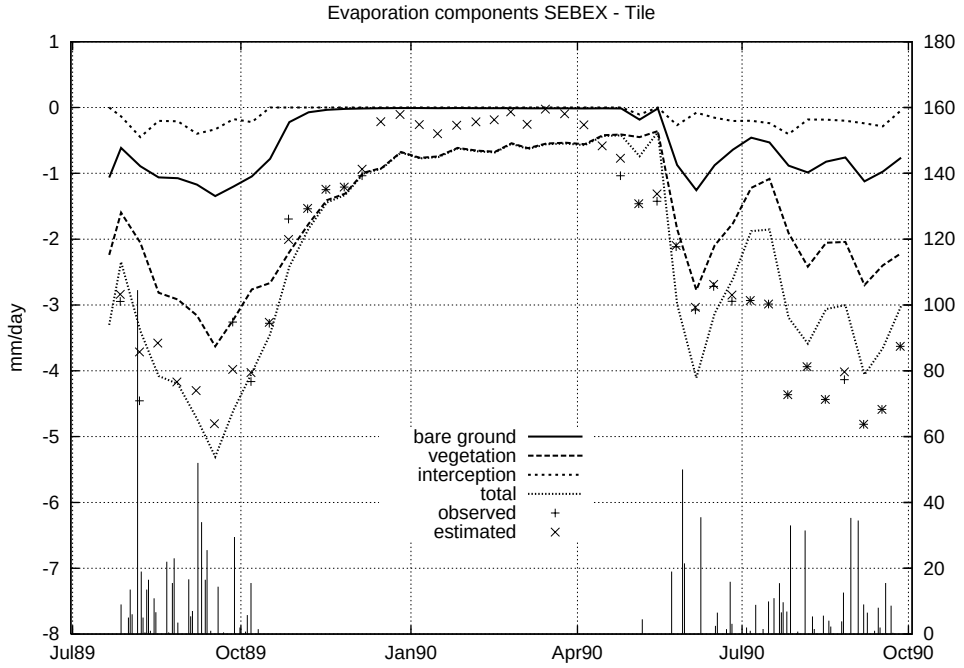

Figure 18: As figure 17, for the tile model.

model has a comparable amount of wet season evaporation, but switches more gradually to a dry season evaporation regime because of the extended rooting depth (figure 18). This gradual evolution corresponds better to the observations. During the dry season, the reduced canopy resistance in the tile model gives higher canopy transpiration. Although the evaporation estimates were obtained rather indirectly, the simulated evaporation in the tile model is probably too high in the dry season, partly because the model has no seasonal vegetation cycle, and partly because the model does not have the correct soil characteristics, as discussed below.

The bare ground evaporation significantly changes the shape of the soil moisture profile in the dry season (figure 19). The water extraction in the tile scheme tends to generate vertically uniform soil water profiles in the absense of rain, whereas steep gradients are simulated in the control scheme. Figure 19 also shows a very large difference between observed and simulated soil moisture contents. Rapid drainage of the coarse textured sandy soil at the site gives very low values of soil moisture in the dry season. The models, with their loamy interpretation of the soil physical properties, hold much higher equilibrium moisture contents, and also show a slower response of soil moisture content to changing precipitation. Soet *et al.* (1999) analyse simulations of a very similar version of the control model as is studied here, guided by atmospheric and hydrological measurements on a nearby site collected during the HAPEX-Sahel campaign in the transition from the wet to the dry season in 1992 (Goutorbe *et al.*, 1994). They used soil water measurements down to nearly 1.75 m depth in combination with recorded rainfall and surface evaporation to conclude that the deep soil percolation in the scheme of VB95 is strongly underestimated. A change of the soil physical properties leading to an increased percolation and lower equilibrium soil moisture contents is necessary to simulate the annual cycle of the Sahelian evaporation.

The difference in prescribed albedo between the tile and control model leads to a reduction of approximately 15 W/m^2 of daily averaged net radiation near the end of the dry season (April-May 1990). Observations suggest that net radiation, while improved, is still too high by another 15 W/m^2 (figure not shown). This net radiation error plays a small role in the (probable) overestimate of dry season evaporation, shown in figure 18.

4.7 Arme

For simulations of the surface energy balance over tropical forest, two changes to the surface scheme appear to play an important role:

- The leaf area index of the dominant canopy type (evergreen deciduous trees, see table 5) has increased from the previous global value of 4 to 6 m^2/m^2. This increases the maximum interception reservoir depth by nearly 50%.

- The minimum canopy resistance has increased from $r_{s,min}/LAI = 272/4$ to $240/6$ s/m, partly offset by an additional stress function (equation 10) for vapour pressure deficit.

These two changes cause a clear increase of both canopy transpiration and interception loss. Figures 20 and 21 show the 10-day averaged evaporation, as distributed over the various grid box fractions. The estimate of total evaporation and evaporation from the interception reservoir, as given by Shuttleworth (1988), is also shown. The increase of the leaf area index

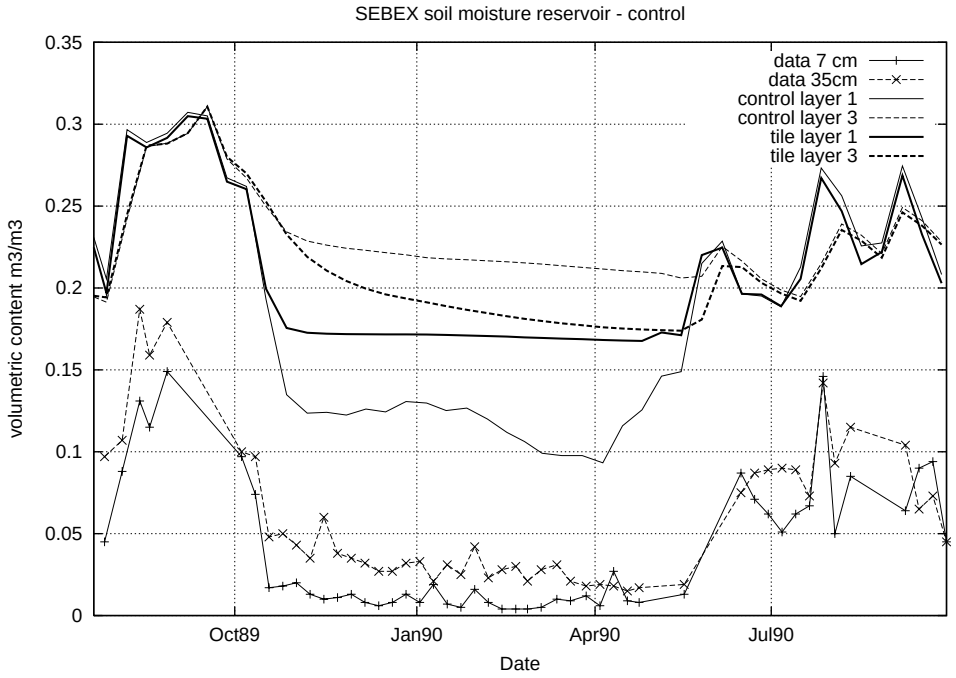

Figure 19: SEBEX measured and simulated soil moisture contents.

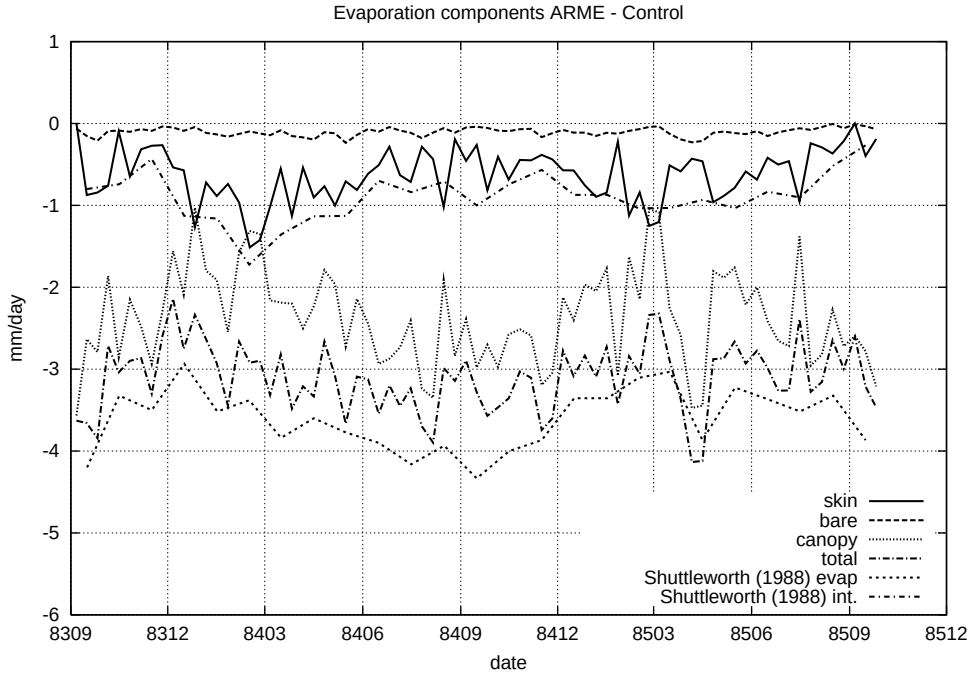

Figure 20: ARME 10-day averaged evaporation from estimates by Shuttleworth (1988) and as simulated by the control model. Shown are separate contributions from the interception reservoir, canopy transpiration and bare ground evaporation.

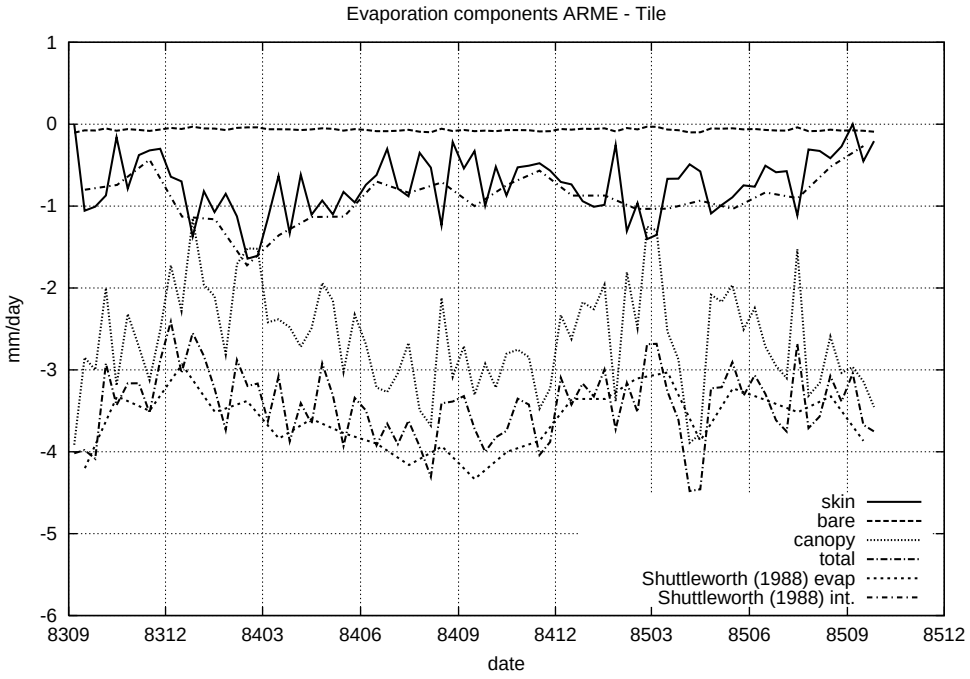

Figure 21: As figure 20, for the tile scheme.

leads to an increase of the interception loss from roughly 8.8 to 10.3% of total precipitation, in close agreement with Shuttleworth (1988). Total evaporation has gone up from 44% to 48%, again close to the estimate of Shuttleworth (1988).

A comparison to direct measurements of evaporative fraction near local noon is shown in figure 22. These direct eddy-correlation data confirm that the tile scheme is superior to the control scheme in the partitioning of daytime available energy into latent and sensible heat.

5 Discussion and conclusions

5.1 Achievements

A new version of the ECMWF land surface scheme was prepared for the 40-year reanalysis (ERA40). The scheme now acknowledges a wide variety of vegetation types, carries a new prognostic snow layer, and applies a tiling approach in calculating a separate energy balance for different subfractions of a model gridbox. Prior to starting the reanalysis cycle, the scheme was tested both using 3-dimensional experiments and by comparing to field observations in an offline mode. Field observations were taken from a wide range of climatological and surface conditions.

We have found a significant improvement of simulated surface turbulent fluxes for the BOREAS site, in particular during periods where snow was present. The improvement is due to the introduction of a separate snow energy budget decoupled from the vegetation and the underlying soil, and the recognition of turbulence and radiative extinction processes between

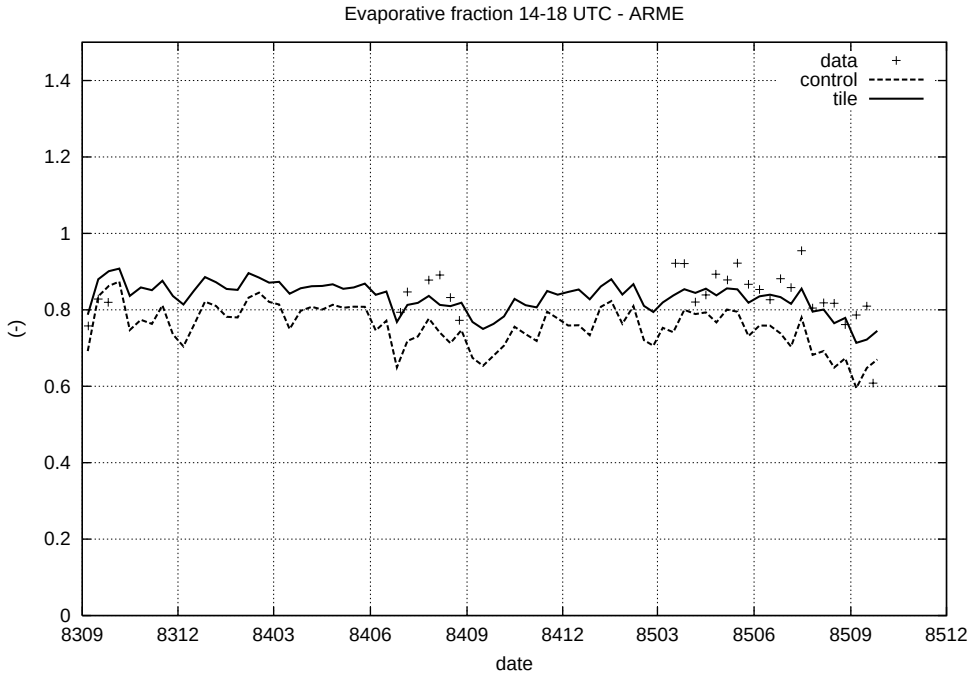

Figure 22: Observed and simulated evaporative fraction between 14:00 and 18:00 UTC for the ARME dataset. Shown are daily averaged observations and 10-day averages of the control and the tile model. Averaging of fluxes is carried out prior to calculating the evaporative fraction.

the snow (lying under the canopy) and the vegetation layer. Most of the available net radiation in winter and spring is now used to heat the atmosphere rather than to evaporate the snow, and this has a beneficial impact on both the surface Bowen ratio and the phasing of snow melt. This improvement has major impact on the simulation of the atmospheric boundary layer and near surface temperature and humidity in the large forested areas on the North American and North Eurasian continents, and will likely feedback to forecasts of precipitation and pressure thickness as well.

The new scheme now differentiates between environmental controls on canopy transpiration for low and high vegetation, which appears supported by observations. Comparison of Cabauw and Garderen simulations shows that forests exhibit a stronger stomatal control than grassland.

Deeper rooting allowed the SEBEX simulation to extend the surface evaporation somewhat longer at a higher level after the rains stop, which is also supported by observations. The transpiration levels in the dry season are however too high compared to estimates by Verhoef *et al.* (1999), and one major cause is an inappropriate choice of soil physical coefficients (see below).

Evaporation simulated for the ARME tropical forest has gone up by 5%, to give better agreement with both on-site eddy-correlation measurements and a calibrated evaporation model by Shuttleworth (1988). The increase of the leaf area index has yielded a more realistic estimation of the interception loss.

The introduction of different vegetation types in the ECMWF model allows a more het-

erogeneous response of evapotranspiration to climate variations. This is a much more realistic approach than the uniform "global grassland" approach followed in the control scheme by Viterbo and Beljaars (1995). It will improve the quality of the surface fields in the new ERA40 cycle, and we hope make the interpretation of the role of (land) surface in the global climate of the recent past more straightforward.

There is a price to be paid for allowing this global variability of vegetation responses, and that is that a large number of parameters have to be estimated (table 1). Although the range of surface conditions included in the 7 datasets used here is fairly wide, still some important global biomes are lacking in this evaluation. No data were available for tundra and arctic surfaces, nor from desert, peat and bog areas, nor for deciduous forest. From the many possible agricultural crop types, only grassland and soybean were represented. This implies that many parameters listed in table 1 have not been carefully evaluated. Some parameters were chosen as a result of the experiments described here. This holds for $r_{s,min}$ and LAI for crops, tall grass and tropical forest, the values of Λ_{sk} for stable and unstable forest interiors (table 2), and the shape of the canopy light stress function (equation 6). For the biomes not included here the parameters were simply copied from literature values, and their validity has yet to be established.

Even with a collection of appropriate datasets available, parameter choice remains a difficult issue. As an example, tall grass was the dominant vegetation type in both the FIFE and SEBEX experiments. The strong response to drought during FIFE prompted the increase in the rooting depth for this vegetation type, whereas the seasonal cycle in SEBEX would suggest to reduce the root reservoir. Necessarily compromises have to be found while selecting appropriate parameter values. Given the impact of the canopy resistance formulation on the seasonal evolution of evapo(transpi)ration in particular, parameter specification is a serious problem in the design of a sophisticated surface scheme for a global model.

The concept of tiling in itself is very appealing. It accounts for the major non-linearities in the surface flux parameterization related to $\partial q_{sat}/\partial T$, stability corrections in C_H and the various evaporation regulation mechanisms. The impact is most pronounced in case of extreme differences between adjacent surface types within a single model gridbox, such as snow near vegetation (see the BOREAS case), or water bodies near land (see e.g. Bringfelt *et al.*, 1999). The concept of tiling the surface energy balance does not seem to lead to major changes of the hydrological budget for a (partially) vegetated surface.

Another attractive feature of the tiling concept is that surface temperatures may be attributed better to local surfaces used for validating the model or assimilating data in it. For instance, satellite derived surface temperatures are usually available at resolutions exceeding significantly the model grid box size, and clearly discern between vegetated and non-vegetated areas. Moreover, surface observations from space are usually only available for cloud-free scenes, and the model structure could easily be extended to discern between a cloudy and a clear-sky surface energy balance. Temperatures from appropriate grid box tiles may thus be compared to the data.

A drawback of the tiling concept is that it decouples gridbox fractions more than sometimes is desirable. For instance, in the real world the evaporation from the interception reservoir is driven by the canopy temperature, and will therefore be accelerated by the warmer dry canopy area as the interception area decreases. This coupling is not present in the current tile model and will possibly lead to an underestimation of the rate of decrease of the interception area.

5.2 Future directions

The testing of the new ERA40 land surface scheme in an offline mode has revealed some remaining unresolved weaknesses in the parameterization. First, the uniform soil physical treatment of water availability, surface runoff and deep water percolation, is unrealistic. This is very clear for the Sahelian sites, where deep water percolation is shown to be strongly underestimated by the model. The HAPEX-Mobilhy results hint in the same direction, while FIFE simulations suggest that the low equilibrium soil water content is at least partially responsible for the underestimation of surface evaporation. This is a complex issue, as it involves both the generation of a representative global map of soil physical properties, and the parameterization of the interplay between surface evaporation, root available water and runoff properties (Koster and Milly, 1997).

Second, the impact of the surface structure on the aerodynamical properties is not yet optimal. Surface roughness plays an important role in the Bowen ratio for interception (Beljaars and Viterbo, 1994) and forest stomatal control (Bosveld and Bouten, 1999b). Also, the calibration of bare ground evaporation using a relative humidity approach as for instance by Mahfouf and Noilhan (1991) relies heavily on a proper estimation of the local roughness length. Yet uniform z_{0m}-values are specified for all tiles in the gridbox. At present, roughness specification in global models is biased towards an optimum momentum budget rather than the heat budget. A tile-dependent roughness length, for instance as listed in table 1, could be included to distinguish between typical aerodynamic features of low and high vegetation. Roughness lengths of heat and momentum should thus be disentangled much further than the current implementation of uniform roughness lengths and roughness ratio's for all tiles.

A third feature which needs additional attention in a future version of the ECMWF surface scheme is the seasonal evolution of vegetation, to be translated into LAI and possible c_{veg} in the model. Simulations for Cabauw, HAPEX-Mobilhy, FIFE and SEBEX indicate that the model's seasonal cycle of evaporation is smaller than in the observations, owing to a clear variation of transpiring surface in the real world. Deciduous forests have not been included in this evaluation, but similar effects can be expected there. Parameter choices as depicted in table 1 are now tuned towards an optimum seasonal hydrological and energy budget, but this could be improved once a seasonality in LAI or c_{veg} is included.

The model evaluation shown in this paper has also made clear that something has changed in the availability of field data. The testing of the control model by VB95 has been executed with only three out of the current seven datasets. Apparently, the call for long term observation records from modellers has resulted in an increased number of these datasets. At present, tens of continuous observation campaigns are operational. Some of these campaigns (e.g. EFEDA, Bolle *et al.*, 1993; NOPEX, Halldin *et al.*, 1999; LITFASS, F. Beyrich, priv.comm.) are designed to satisfy the need for an estimate of the surface fluxes at the horizontal scale of a typical GCM gridbox. On the other hand, the practical availability of some of these datasets is not yet optimal: some are unreported in the open literature, some are unavailable to non-participants or perhaps just unknown to us. A central databank for these datasets would be a very welcome initiative.

Acknowledgements Model evaluation is critically dependent on the availability of (long term) data sets. The authors are extremely grateful to the science teams of BOREAS, HAPEX-

Mobilhy, FIFE, ARME, SEBEX and KNMI (operating the Cabauw and Garderen experiments), for making the data available and critically responding to questions. In particular, efforts by Fred Bosveld (KNMI), Simon Allen and Anne Verhoef (Institute of Hydrology), John Ball (Atmospheric Research) and Jean-Francois Mahfouf (ECMWF) are appreciated. Xubing Zeng (University of Arizona) advised on the specification of root profiles, which is gratefully acknowledged. The first author was partially sponsored by the Dutch National Research Program NRSP-2 under contract nr 951246. The 4^{th} author was supported by NSF under grant ATM9505018, and NASA under grant NAS5-7377.

References

Beljaars, A.C.M. and F.C. Bosveld (1997): Cabauw data for the validation of land surface parameterization schemes; *J. Clim.* **10**, 1172-1193.

Beljaars, A.C.M. and A.A.M. Holtslag (1991): Flux parameterization over land surfaces for atmospheric models; *J. Appl. Meteor.* **30**, 327-341

Beljaars, A.C.M. and P. Viterbo (1994): The sensitivity of winter evaporation to the formulation of aerodynamic resistance in the ECMWF model; *Bound.-Layer Meteor.* **71**, 135-149.

Betts, A.K. and J.H. Ball (1998): FIFE surface climate and site-averaged dataset 1987-89; *J. Atmos. Sci.* **55**, 1091-1108.

Betts, A.K., P. Viterbo, and E.F. Wood (1998a): Surface energy and water balance for the Arkansas-Red river basin from the ECMWF reanalysis; *J. Clim.* **11**, 2881-2897.

Betts, A.K., P. Viterbo, A. Beljaars, H.-L. Pan, S.-Y. Hong, M. Goulden and S. Wofsy (1998b): Evaluation of land surface interaction in ECMWF and NCEP/NCAR reanalysis models over grassland (FIFE) and boreal forest (BOREAS); *J. Geophys. Res.* **103**, 23079-23085.

Betts, A.K., P. Viterbo and A.C.M. Beljaars (1998c): Comparison of the land-surface interaction in the ECMWF Reanalysis model with the 1987-FIFE data; *Month. Weather Rev.* **126**, 186-198.

Betts, A.K., M. Goulden and S. Wofsky (1999): Controls on evaporation in a boreal spruce forest; *J. Clim.* **12**, 1601-1618.

Betts, A.K. and P. Viterbo (2000): Hydrological budgets and surface energy balance of seven subbasins of the Mackenzie river from the ECMWF model; *J. Hydrometeor.* (in press).

Bolle, H.-J., and Co-Authors (1993): EFEDA: European field experiment in a desertification-threatened area; *Annales Geophysicae* **11**, 173-189.

Bonan, G.B. (1994): Comparison of two land surface process models using prescribed forcings; *J. Geophys. Res.* **99D**, 25803-25818.

Bosveld, F.C. (1997): Derivation of fluxes from profiles over a moderately homogeneous forest; *Bound.-Layer Meteor.* **84**, 289-327.

Bosveld, F., A. van Ulden and A. Beljaars (1998): A comparison of ECMWF re-analysis data with fluxes and profiles observed in Cabauw; ECMWF ERA-project Series No 7.

Bosveld, F.C., A.A.M. Holtslag and B.J.J.M. van den Hurk (1999): Nighttime convection in the interior of a dense Douglas fir forest; in press by *Bound.-Layer Meteor.*.

Bosveld, F.C. and W. Bouten (1999a): Evaporation and transpiration reduction of a partially wet Douglas-fir forest; submitted to *Agric. Forest Meteor.*

Bosveld, F.C. and W. Bouten (1999b): Evaluation of transpiration models with observations over a Douglas fir forest; submitted to *Agric. Forest Meteor.*

Bringfelt, B., N. Gustafsson, V. Perov, A. Lindroth and M. Heikinheimo (1999): A new land surface treatment for Hirlam - comparisons with Nopex measurements; in press by *Agric. Forest Meteor.*

Chen, T.H. and Co-Authors (1997): Cabauw experimental results from the project for inter-comparison of land-surface parameterization schemes; *J. Clim.* **10**, 1194-1215.

Clapp, R.B., and G.M. Hornberger (1978): Empirical equations for some soil hydraulical properties; *Water Resources Res.* **14**, 601-604.

Claussen, M., Lohmann, U., Roeckner, E. and Schulzweida, U. (1994): *A global dataset of land-surface parameters*; Max-Planck-Institut fur Meteorologie, Hamburg, 23 pp.

Dickinson, R.E., A. Henderson-Sellers, P.J. Kennedy (1993): *Biosphere-Atmosphere Transfer Scheme (BATS) for the NCAR Community Climate model*; NCAR Technical Note NCAR/TN-275+STR, 72 pp.

Dorman, J.L. and P.J. Sellers (1989): A global climatology of albedo, roughness length and stomatal resistance for atmospheric general circulation models as represented by the Simple Biosphere Model (SiB); *J. Appl. Meteor.* **28**, 833-855.

Douville, H. J.-F. Royer and J.-F. Mahfouf (1995): A new snow parameterization for the Meteo-France climate model. Part I: validation in stand-alone experiments; *Clim. Dynamics* **12**, 21-35.

Douville, H., J.-F. Mahfouf, S. Saarinen and P. Viterbo (1998): *The ECMWF surface analysis: diagnostics and prospects*; ECMWF Techn.Memo. 258, 51 pp.

Ek, M. and A.A.M. Holtslag (1999): Interaction of the atmospheric boundary-layer with the land surface: a case study at Cabauw; Proceedings AMS Symposium on boundary layers and turbulence.

Giard, D. and E. Bazile (1999): Implementation of a new assimilation scheme for soil and surface variables in a global NWP model; Submitted *Month. Weather Rev.*

Goulden, M.L., B.G. Daube, S.-M. Fan, D.J. Sutton, A. Bazzaz, J.W. Munger and S.C. Wofsy (1998): Physiological responses of a black spruce forest to weather; *J. Geophys. Res.* **D102**, 28987-28996.

Goutorbe, J.-P. (1991): *A critical assessment of the* SAMER *network accuracy*; In: Land surface Evaporation; Ed. by Schmugge and André; Springer-Verlag, pp. 403-410.

Goutorbe, J.-P., and Co-Authors (1994): HAPEX-Sahel: a large scale study of land atmosphere interactions in the semi-arid tropics; *Annales Geophysicae* **12**, 53-64.

Hagemann, S. and L. Dümenil (1999): *Validation of the hydrological cycle and computation of discharge from ECMWF and NCEP reanalyses*; 2nd International Conference on Reanalyses, 23 to 27 August 1999, Wokefield Park, Mortimer, Reading, UK.

Halldin, S., L. Gottschalk, S.-E. Gryning, A. Jochum, L.-C. Lundin and A.A. Van de Griend (1999): Energy, water and carbon exchange in a boreal forest landscape - NOPEX Experiments; in prep.

Henderson-Sellers, A., Z.-L. Yang and R.E. Dickinson (1993): The Project for Intercomparison of Land-surface Intercomparison Schemes; *Bull. Am. Meteor. Soc.* **74**, 1335-1349.

Jarvis, P.G. (1976): The interpretation of the variations in leaf-water potential and stomatal conductance found in canopies in the field; *Philos. Trans. Roy. Soc. London* **B723**, 593-610.

Koster, R.D. and M.J. Suarez (1992): Modeling the land surface boundary in climate models as a composite of independent vegetation stands; *J. Geophys. Res. (D)* **97**, 2697-2715.

Koster, R.D. and P.C.D. Milly (1997): The interplay between transpiration and runoff formulations in land surface schemes used with atmospheric models; *J. Clim.* **10**, 1578-1591.

Mahfouf, J.-F. (1990): A numerical simulation of the surface water budget during HAPEX-Mobilhy; *Bound.-Layer Meteor.* **53**, 201-222.

Mahfouf, J.F. and J. Noilhan (1991): Comparative study of various formulations of evaporation from bare soil using in situ data; *J. Appl. Meteor.* **30**, 1354-1365.

Mahfouf, J.-F., A.O. Manzi, J. Noilhan, H. Giordani and M. Deque (1995): The land surface scheme ISBA within the Meteo-France climate model ARPEGE. Part I: Implementation and Preliminary results; *J. Clim.* **8**, 2039-2057.

Manzi, A.O., and S. Planton (1994): Implementation of the ISBA parametrization scheme for land surface processes in a GCM - an annual cycle experiment; *J. Hydrol.* **155**, 353-387

Peters-Lidard, C.D., M.S. Zion, and E.F. Wood, 1997: A soil-vegetation-atmosphere transfer scheme for modeling spatially variable water and energy balance processes; *J. Geophys. Res.* **D102**, 4303-4324.

Pitman, A.J., Z.-L. Yang, J.G Cogley, and A. Henderson-Sellers (1991): *Description of bare essentials of suface transfer for the Bureau of Meteorology Research Centre AGCM*; Bur. Meteor. Res. Rep. No.32, 86pp.

Sellers, P. J. and Co-Authors (1998): BOREAS in 1997: Experiment overview, scientific results and future directions. *J. Geophys. Res.* **D102**, 28731-28769.

Shao, Y., R.D. Anne, A. Henderson-Sellers, P. Irannejad, P. Thornton, X. Liang, T.H. Chen, C. Ciret, C. Desborough, O. Balachova, A. Haxeltine and A. Ducharne (1994): *Soil moisture simulation - a report of the RICE and PILPS Workshop*; IGPO Publ. Series No 14, Clim.Impact Centre, 179 pp.

Shewchuk, S. (1998): Surface mesonet for BOREAS; *J. Geophys. Res.* **D102**, 29077-29082.

Shuttleworth, W.J., and Co-Authors (1984): Eddy correlation measurements of energy partition for Amazonian forest; *Q. J. Roy. Meteor. Soc.* **110**, 1143-1162.

Shuttleworth, W.J. (1988): Evaporation from Amazonian rainforest; *Proc. R. Soc. Lond.* **233**, 321-346.

Soet, M., R.J. Ronda, J.N.M. Stricker and A.J. Dolman (1999): Model conceptualisation and standard parameter values in a one-dimensional land surface scheme; Submitted to *J. Appl. Meteor.*

Tiktak, A. and W. Bouten (1994): Soil water dynamics and long-term water balances of a Douglas fir stand in the Netherlands; *J. Hydrol.* **156**, 265-283.

USGS (1999): see `http:edcwww.cr.usgs.gov/landdaac/glcc/glcc.html`.

Van den Hurk, B.J.J.M. and A.C.M. Beljaars (1996): Impact of some simplifying assumptions in the new ECMWF-surface scheme; *J. Appl. Meteor.* **35**, 1333-1343.

Verhoef, A., S.J. Allen and C.R. Lloyd (1999): Seasonal variation of surface energy balance over two Sahelian surfaces; In press by *Int. J. Climatology.*

Viterbo, P. (1994): *Initial values for soil moisture*; Memorandum ECMWF research department, R60.6.1/PV/204

Viterbo, P. and A.C.M. Beljaars (1995): An improved land surface parametrization scheme in the ECMWF model and its validation; *J. Clim.* **8**, 2716-2748.

Viterbo, P. and P. Courtier (1995): *The importance of soil water for medium-range weather forecasting. Implications for data assimilation.* WMO workshop on Imbalances of slowly varying components of predictable atmospheric motions, Beijing, China, March 1995; WMO/TD 652, pp. 121-130.

Viterbo, P. and A.K. Betts (1999): The forecast impact of changes to the albedo of the boreal forests in the presence of snow; *J. Geophys. Res.* **104**, 27803-27810.

Viterbo, P., A. Beljaars, J.-F. Mahfouf and J. Teixeira (1999): The representation of soil moisture freezing and its impact on the stable boundary layer; *Q. J. Roy. Meteor. Soc.* **125**, 2401-2426.

Viterbo, P. and Co-Authors (2000): Revision of the ECMWF surface scheme; (in preparation).

Wallace, J.S., I.R. Wright, J.B. Stewart and C.J. Holwill (1991): The Sahelian energy balance experiment (SEBEX): ground based measurements and their potential for spatial extrapolation using satellite data; *Adv. Space Res.* **11**, 31-41.

Zeng, X., Y-J. Dai, R.E. Dickinson and M. Shaikh (1998): The role of root distribution for land climate simulation; *Geophys. Res. Letters* **25**, 4533-4536.